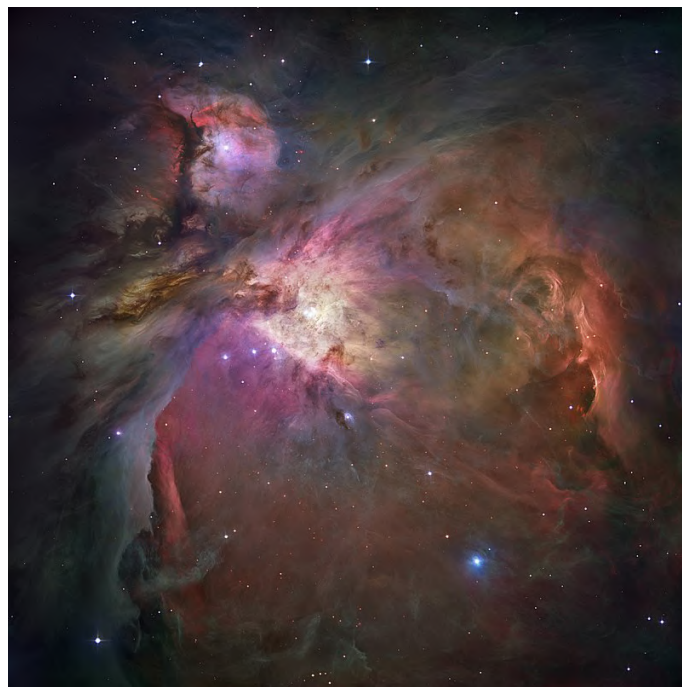

M2 internship report :

Formation of water in presence of CO on interstellar dust grains



Basile HUSQUINET

*M2 Fundamental Physics
Aix-Marseille University*

Supervisor : Pr. François DULIEU (Professor and Laboratory Director)

*Laboratoire d'Etudes du Rayonnement et de la Matière en Astrophysique et
Atmosphères pôle de Cergy Université (CY-LERMA)*

10 janvier 2023

Table des matières

1	Introduction	5
2	Background	6
2.1	Surface Physics	6
2.1.1	Adsorption	6
2.1.2	Desorption	6
2.2	Surface Chemistry	8
3	Experimental apparatus and method	10
3.1	Experimental apparatus	10
3.1.1	Ultra High Vacuum system	11
3.1.2	The sample holder and cryostat	11
3.1.3	The beamline system	12
3.1.4	Quadrupole Mass Spectrometer (QMS)	12
3.1.5	Fourier transform Infrared (FT-IR) spectrometer	13
3.2	Experimental methods	14
3.2.1	Optimization of the beam flux	14
3.2.2	Temperature Programmed Desorption (TPD)	14
3.2.3	Dissociation of H_2	16
3.2.4	Cracking pattern	17
4	Prior experiment	18
4.1	Formation of water	18
4.1.1	The possible reaction	18
4.1.2	Co-deposition of O ₂ and H	19
4.2	Formation of methanol	21
4.2.1	The possible reaction	21
4.2.2	Co-deposition of CO and H	22
4.3	The gas phase	24
5	Formation of water in presence of CO	27

6 Indirect chemical desorption	31
7 Conclusion	34

Acknowledgements

First of all I would like to thank Patrice Theulé for having introduced me to Astrochemistry and for taking care of me throughout this master. Moreover I really want to thank you for having given me the opportunity to do my master 2 internship in the CY-LERMA laboratory under the supervision of François Dulieu and for having found me a thesis opportunity.

Then I would like to thank François Dulieu for having guided me and having trusted me for his M2 physics internship. I have to thank you again for giving me your confidence to pursue this project in thesis with Paola Caselli that I thank for giving me her confidence.

I would like to thank all the CY-LERMA team, for the good atmosphere and all the help I received during the internship, especially Saoud Baouche and Laurent Nussbaum with all the problems I had during the month of May on VENUS. A special thanks to Julie Vitorino for teaching me how to use VENUS and all the help I received during the internship and on this report

I also thank my friends of the master in particular Kateriniovi, Salomé Grouffal, Jade Piat, Thomas Muller and especially Thomas Lucet for all the help, moral support, great conversation on physics and astrophysics, on our night of observation and so on.... Just thank you very much without you I wouldn't have made it to the end.

Resumé en Français

L'astrophysique en laboratoire permet de reproduire des conditions de températures et de pression similaire aux milieux interstellaires, c'est-à-dire une pression avoisinant 10^{-11} mbar et une température de 10K. Toutes les expériences au CY-LERMA ont été réalisées avec VENUS qui est capable de reproduire ses conditions. Le méthanol est la molécule la plus représentative des molécules organiques complexes (COMs) et sert de référence en matière d'abondance pour toutes les autres COMs. Cependant sa formation n'est pas encore totalement comprise et de même que sa présence en phase gazeuse dans les nuages sombres. Nous avons étudié comment le ratio H_2O_2/H_2O varie avec la présence de CO lors d'une codeposition de CO , O_2 et H . Nous avons vu que le CO empêche la bonne hydrogénation de O_2 ce qui donne un ratio $H_2O_2/H_2O \approx 1$. De plus la présence de méthanol par hydrogénation du CO est insignifiante $> 1\%$ du CO déposé. Cependant nous avons pu mettre en évidence un nouveau procédé de désorption chimique nommée désorptions chimiques indirectes. L'excès d'énergie de la réaction $OH + H$ se diffuserait à ses voisins qui ne serait pas capable de dissiper cette énergie et donc serait éjecté de la surface. Pour le CO et O_2 ça représenterait de l'ordre de 30 à 50%. Cette désorption chimique indirecte nous aide à comprendre la présence de méthanol en phase gazeuse dans le nuage sombre.

Abstract in English

Laboratory astrophysics allows to reproduce temperature and pressure conditions similar to interstellar environments, i.e. a pressure of about 10^{-11} mbar and a temperature of 10K. All the experiments at CY-LERMA were performed with VENUS which is able to reproduce these conditions. Methanol is the most representative molecule of the complex organic molecules (COMs) and serves as a reference in abundance for all other COMs. However, its formation is not yet fully understood and neither is its presence in the gas phase in dark clouds. We have studied how the ratio H_2O_2/H_2O varied with the presence of CO during a codeposition of CO , O_2 and H . We have seen that CO prevents the good hydrogenation of O_2 which gives a ratio $H_2O_2/H_2O \approx 1$. Moreover the presence of methanol by hydrogenation of CO is insignificant $> 1\%$ of the CO deposited. However, we have been able to demonstrate a new chemical desorption process called indirect chemical desorption. The excess energy of the $OH + H$ reaction would diffuse to its neighbors which would not be able to dissipate this energy and thus would be ejected from the surface. For CO and O_2 this would represent about 30 to 50%. This indirect chemical desorption helps us to understand the presence of methanols in gas phase in the dark cloud.

1 Introduction

The interstellar medium is the most fascinating object in the universe. Representing $\sim 10\%$ of the mass of baryonic matter and according to 0.2% of the estimated total mass of the universe [1]. It is the most important component of galaxies and is responsible for the formation of stars, which are great sources of energy and heavy element creation. Due to gravitation, the ISM is not homogeneous with different regions of varying pressure and temperature. These regions vary from the coronal gas surrounding the stars which is very low density 0.004 cm^{-3} but with an average temperature of 10^6 K , to the dense molecular clouds which have an average temperature of 10 K but a density ranging from 10^3 to 10^6 cm^{-3} [2]. Due to their very high hydrogen density and dust, dense molecular clouds are protected from the UV radiation of stars, allowing for the highest chemical activity in the Universe. However, even being protected from UV, the density present should not allow for very complex chemistry to occur. It is the presence of interstellar dust that acts as a chemical catalyst. This interstellar dust represents only 1% of the mass of ISM.

The most abundant reaction on interstellar dust grains is the recombination of hydrogen [3]. However, a much more complex chemistry is present which forms molecules called interstellar Complex Organic Molecules (iCOM) so that 6 molecules have been observed for sure on interstellar ices of which the most representative iCOM is the methanol CH_3OH . The other molecules are H_2O , CO_2 , CO , NH_3 and CH_4 . Many other are suspected (H_2CO , H_2O_2 , HCOOH , ...) [4]. For the last 20 years, methanol has been one of the most studied molecules. Due to its ease of observation, its rich spectrum and being the icon of COMs it is a target of choice for Astrochemists. However, many questions remain, including its presence in the gas phase. Theoretically, methanol can only be formed on grains and with temperatures around 10 K , all molecules should condense on the grain within a short time [5] but methanol has been observed in the gas phase under these conditions [6][7][8].

In this internship, we were particularly interested in the formation of water in the presence or absence of CO . Based on the work of Oba et al. (2009) [9], we studied the formation of water in interstellar mediums, i.e. how the $\text{H}_2\text{O}_2/\text{H}_2\text{O}$ ratio varies according to the oxygen and hydrogen fluxes and how to maximize H_2O formation. In addition, we studied the formation of water in the presence of CO and thus the amount of methanol produced under these conditions. Finally, in the experiments, we suspect a new type of chemical desorption that could partly explain the presence of methanol and others molecules in the gas phase in dark clouds.

This report is organized as follows, in section 2 we look at the basic theory of surface physics and chemistry, in section 3 we describe the VENUS set-up used at CY-LERMA and the experimental method, preliminary experiments on the formation of water and methanol are described in section 4, in section 5 the formation of water in the presence of CO is studied and finally in section 6 we discuss the new type of chemical desorption used in our experiments.

2 Background

This part is inspired by the book "*Molecular astrophysics*" of A.G.G.M Tielens published in 2021 [10], the thesis of M. Minissale [11] and the thesis of T. Nguyen [12].

2.1 Surface Physics

2.1.1 Adsorption

The dark clouds have temperatures close to $10K$ for gas and grains. At this temperature, the chemical species in the gas phase have a probability of sticking to the surface of the grain during a collision with it close to 1. This effect is called adsorption. There are two types of adsorption: physisorption and chemisorption. Figure 2.1 illustrates these two mechanisms. Physisorption adsorption sites correspond to a rather weak minima in the potential energy (about $\sim 10 - 400meV$ or $100 - 5000K/k_B$). Physisorption represents the van der Waals bonds of the chemical species with the surface. The van der Waals bond is described by the potential of Lennard-Jones potential at the equation 2.1

$$U(r) = D_\epsilon \left[\left(\frac{\sigma}{r} \right)^{12} - \left(\frac{\sigma}{r} \right)^6 \right] \quad (2.1)$$

where D_σ defines the strength of the potential, σ is its range and r the distance between the particle and the surface. Analytically, the repulsion is described by the term in r^{-12} and the attraction by the term in r^{-6} . Physisorption is the most common non-reactive particle-surface bond on grains. Chemisorption has a much higher energy ($1 - 10eV$) and corresponds to covalent bonding of the chemical species with the surface. It is described in the equation 2.2 by the Morse potential:

$$U(r) = D_\epsilon [1 - e^{-\alpha(r-r_e)}] \quad (2.2)$$

where D_ϵ defines the strength of the potential, α is its range and r_e the equilibrium distance. For chemisorption to occur, most of the time, the environment must be very energetic (mean temperature close to $600K$). This would correspond for example to the chewing of a meteorite on celestial bodies. In the present experiments, we will never have enough energy to have chemisorption with the underlying substrate.

2.1.2 Desorption

In this report, we will mainly consider two types of desorptions: the thermal desorption and the chemical desorption. Thermal desorption corresponds to the ejection of molecules from the surface by increasing its temperature. By knowing the temperature at which the

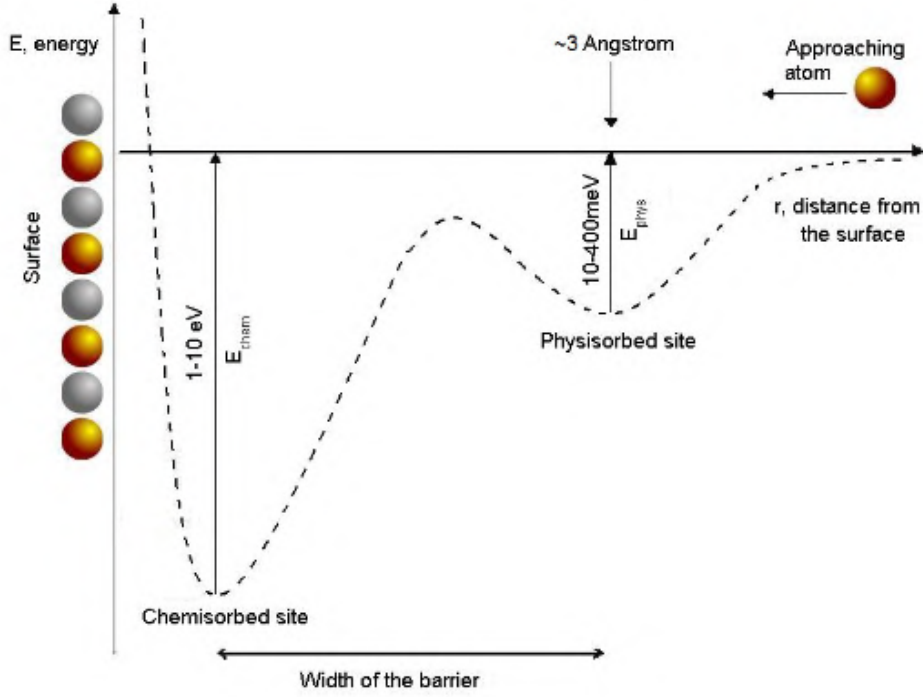


Figure 2.1 – Diagram of the potential energy of the adsorption as a function of the distance to the surface.[11]

molecules desorb, we can estimate their binding energy with the surface. Using the Arrhenius law¹, Polanyi-Wigner gives us an equation that links the number of molecules that desorb as a function of temperature.

$$r(N, E_b, T) = -\frac{dN}{dt} = AN^n e^{-E_b/k_B T} \quad (2.3)$$

where N is the total number of particles adsorbed, E_b is the binding energy in $kJ\ mol^{-1}$, T the temperature in K , n the order of the desorption kinetics, A the desorption efficiency factor in s^{-1} and k_B the Boltzmann constant, $k_B = 1.38064910^{-23}\ J\ K^{-1}$. The thermal desorption is used in the experiments to measure the number of molecules adsorbed on the surface as we will see in more details in the section 3.2.2. When molecules react with each other to form a new product, the reaction may be endothermic, meaning that it absorbs energy from the environment, or exothermic. When the reaction is exothermic, the new molecule may not be able to dissipate the excess energy on the surface, and so may be ejected from it. This effect is called chemical desorption[14][13]. Figure 2.2 comes from the article by Dulieu et al. (2013)[13] and summarizes the chemical desorption.

1. Arrhenius' law links the speed of a chemical reaction to the temperature. $\frac{d \ln k}{dT} = \frac{E_a}{RT^2}$ where k is the velocity coefficient, T the temperature, E_a Activation energy and R the perfect gas constant.

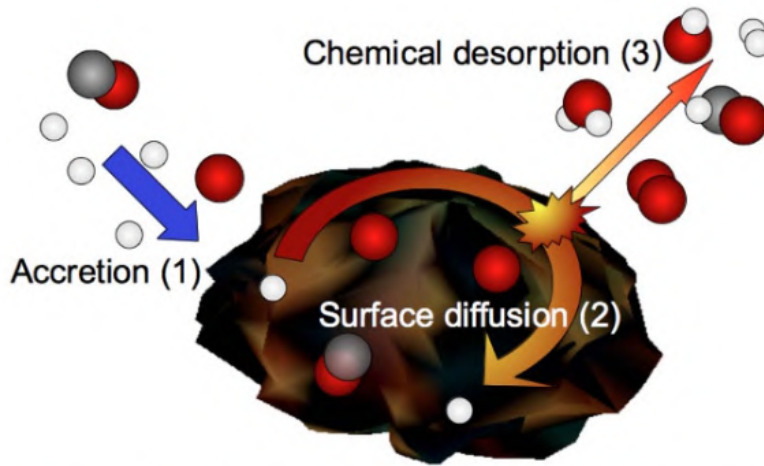


Figure 1 | Sketch that illustrates the chemical desorption process. Species coming from the gas accrete on the dust surface and can meet each other to form other species. For some reactions shown in this study, the formed product is ejected in the gas.

Figure 2.2 – Sketch of chemical desorption process on an interstellar grain surface.[13]

2.2 Surface Chemistry

Chemical reactions in molecular clouds take place mainly on the surface of interstellar dust grains. Wakelam et al. (2017)[15] summarized the known effects on surface physics and chemistry. They highlighted five physico-chemical effects which are described in figure 2.3. The first, the Sticking effect is described in the previous section.

The second is the diffusion effect. When a chemical species is adsorbed on an energy site, it is possible that it moves either by jumping over the energy barrier thanks to thermal agitation (solid red arrow) or by tunnel effect (dotted red arrow). Moreover, by diffusing, they can go to less energetic sites, which allows them to better resist desorption [16].

Third, we have the mechanisms that allow chemistry to take place

- Langmuir-Hinshelwood (LH) mechanism: the chemical species diffuse across the surface until they chemically bond together. The diffusion phenomenon can be both jumping and tunneling. It is possible that chemical desorption occurs during the reaction.
- Eley-Rideal (ER) mechanism: One chemical species is adsorbed on the surface and the other chemical species reacts directly with it coming from the gas phase.
- Harris-Kasemo (Hot-atom) mechanism: A chemical species in the gas phase collides with the surface. The excess energy of the collision prevents it from being adsorbed and the chemical species bounces off the surface until it reacts with another already adsorbed.

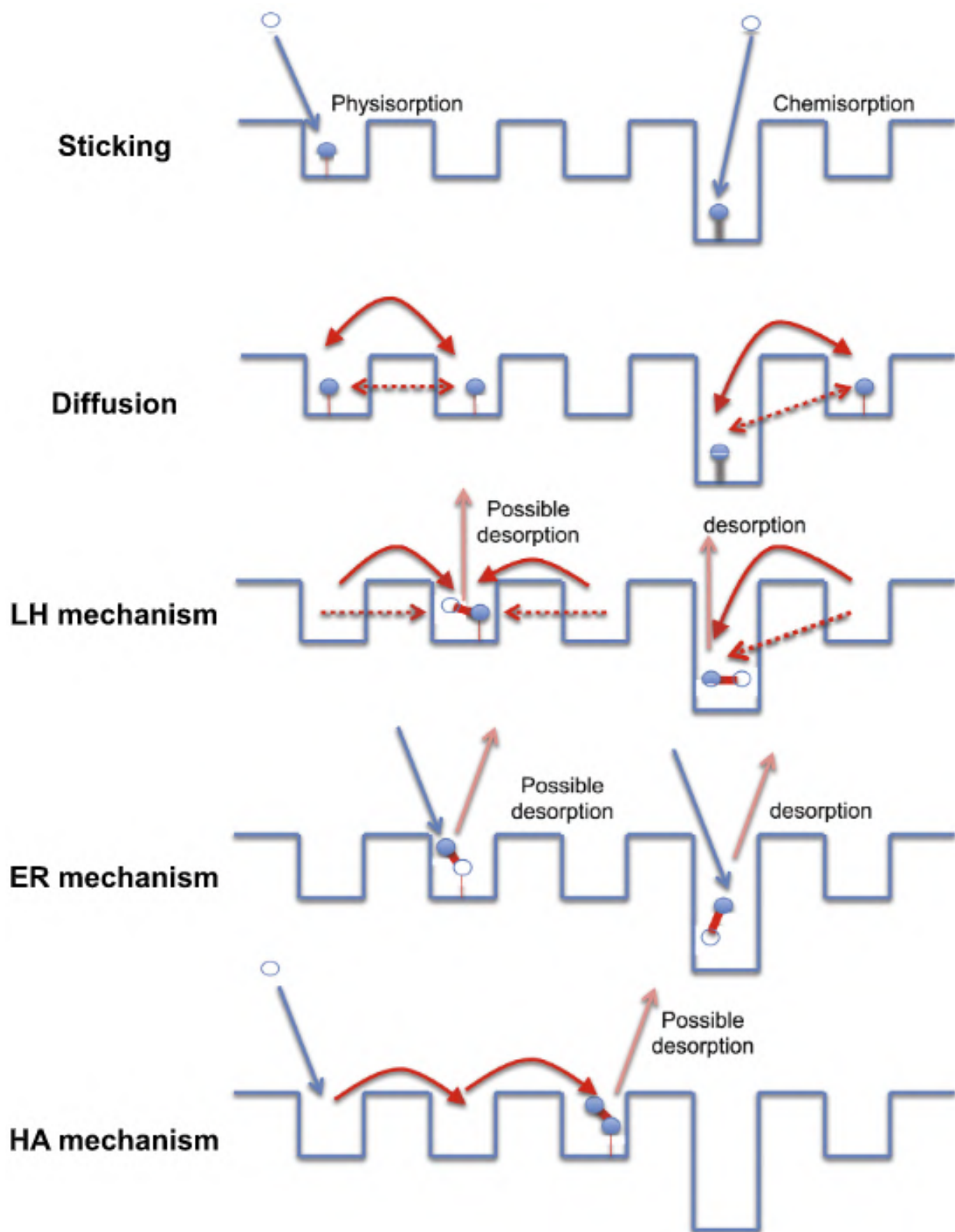


Figure 2.3 – Sketch of surface process. Credit: [15]

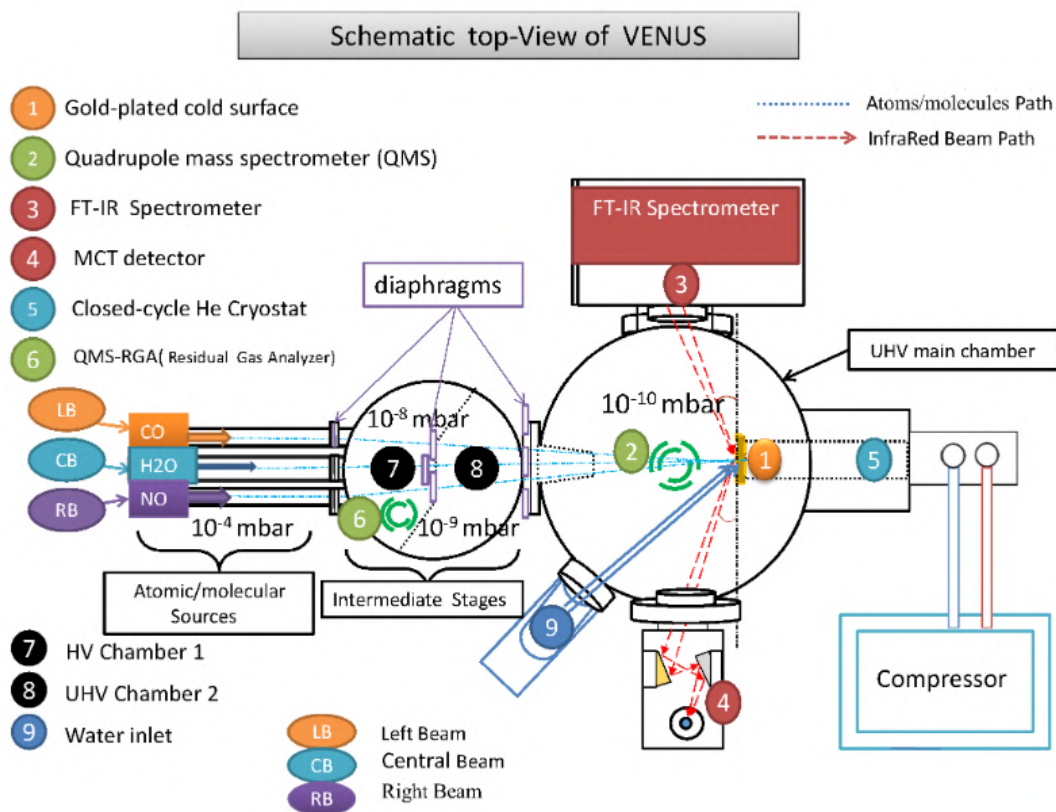


Figure 3.1 – Schematic view of VENUS. Credit: [17]

3 Experimental apparatus and method

The experiments were conducted with the VENUS (VErs de NoUvelle Synthèse) set-up described in more details elsewhere [17] [12].

3.1 Experimental apparatus

Figure 3.1 describes the set-up. It consists of different parts:

- An Ultra High Vacuum (UHV) chamber called main chamber
- Two chambers (1 and 2) used as intermediate pumping stages
- A separated four-beamlines system to inject molecules (or atoms) towards the sample located in the main chamber
- A sample holder connected to the cryostat in the main chamber
- An Infrared spectrometer used at grazing angle to maximize the column density of molecules probed (FT-RAIRS)
- A Quadruple Mass Spectrometer connected in the main chamber that can be moved in front of the sample
- A beam for water molecules, directly connected to the main chamber

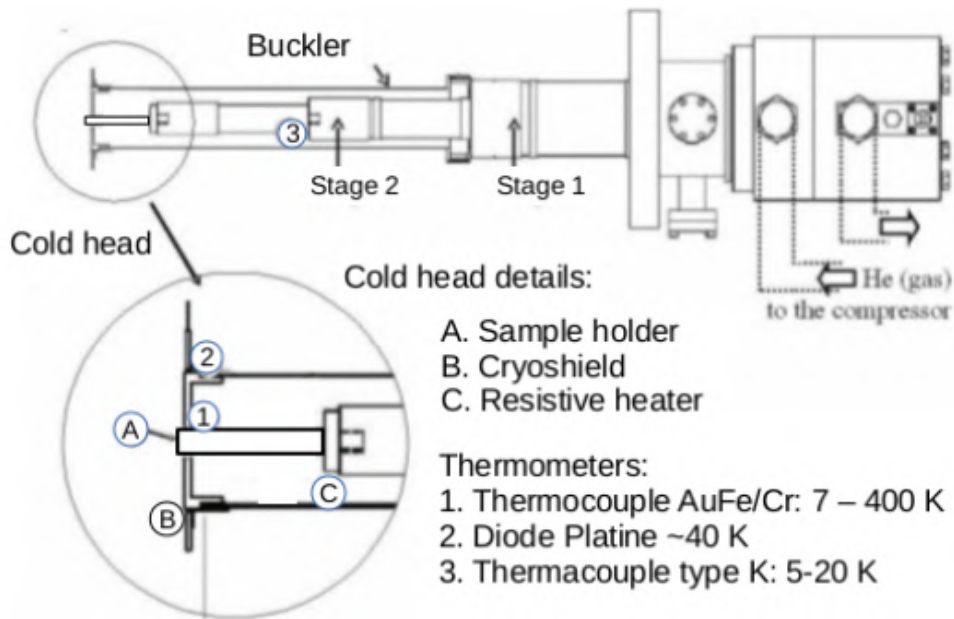


Figure 3.2 – A schematic view of the Cryostat. Credit: [12]

3.1.1 Ultra High Vacuum system

The main chamber is a Ultra High Vacuum (UHV) system. It consists of a stainless steel enclosure connected to a turbo pump and a titanium sublimation pump which allows to have a residual pressure of $1 \times 10^{-10} \text{ mbar}$, corresponding to a molecular/atomic density of about $2 \times 10^6 \text{ cm}^{-3}$. Going down to lower pressures (closer to the interstellar medium $\sim 10^{-13} \text{ mbar}$) would not be a good idea because, technologically, it is very difficult and if we could, the experiments would take several months or years. With the pressure of 10^{-10} mbar and a sample temperature of 10 K , the sample-holder is coated with $\sim 1 \text{ ML}$ of water vapor after only ~ 5000 minutes [18]. If we look at the figure 3.1, the main chamber is connected of two intermediary chamber. Chamber 2 (CH2) is connected directly to the main chamber and has a pressure of 10^{-9} mbar . The Chamber 1 (CH1) is in the middle of the beamline and chamber two, it has a pressure of 10^{-8} mbar . This pressure gradient allows the beam to be directed towards the main chamber on the sample.

3.1.2 The sample holder and cryostat

The sample is in the main chamber and connected on the cryostat. The sample holder is an Oxygen-Free High Conductivity (OFHC) copper cylinder mirror covered in gold. The diameter of the cylinder is 9 mm where the beams have a diameter of 3 mm . A cryocooler is mounted at the end of the sample with a closed cycle *He* cryostat. Right next to the sample is installed a resistor that allows to modify the temperature of the sample with a range from 6 to 400 K . Around the sample is a shield to avoid damage to the cryostat system. The figure 3.2 is a sketch of the sample holder and cryostat system.

3.1.3 The beamline system

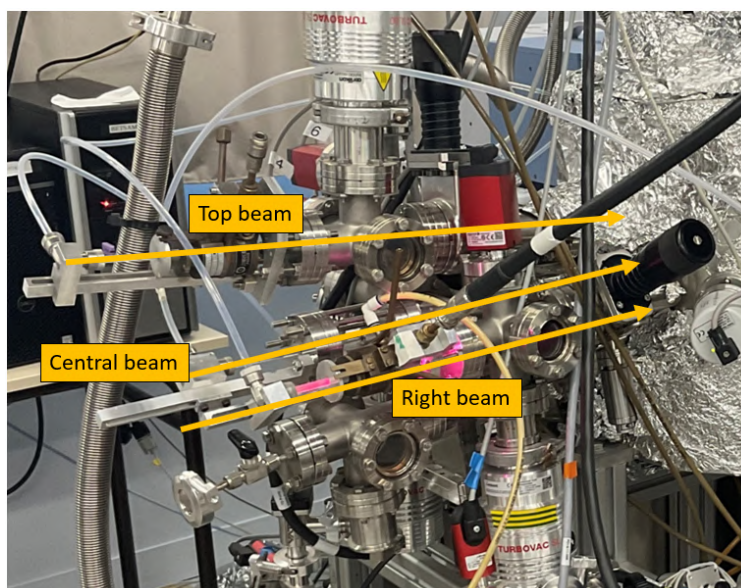


Figure 3.3 – Picture of The separated four-beamline system

The separated four-beamline system allows different chemical species to be deposited on the sample at the same time. The figure 3.3 show a picture of the beamline system of VENUS, it is represented the right, central and the top beam. The bottom beam is not shown because it was soldered at the wrong angle during the manufacture of VENUS. It is not aligned with the other beams so it is not used. A series of diaphragms are placed from the beams to the main chamber to focus the beams on the surface and not impact the residual pressure of the chamber.

3.1.4 Quadrupole Mass Spectrometer (QMS)

The QMS is a spectrometer that measures the mass of atoms and molecules. During an experiment, it allows us to study the composition and abundance of molecules on the surface during the Temperature Programmed Desorption (TPD). Moreover, on VENUS, the QMS is placed just in front of the surface (figure 3.4 in the left panel) which allows us to test the composition of our beam and to measure their flow.

Figure 3.4 in left panel is a diagram of the QMS operation. A QMS consists of a tungsten filament in the head which allows to ionize the gas by bombarding it with electrons, an ion accelerator, a mass filter in the body of the QMS which consists of four parallel rods and a detector at the end. The mass filter selects species according to their mass-to-charge ratio (m/z); in fact, a voltage combination of a direct and a radio frequency component is applied between adjacent and opposite rods. Varying the direct and the radio frequency component, the QMS is capable of scanning all ions up to a chosen mass to charge ratio technically fixed. The QMS is mounted in the bottom part of the main chamber figure 3.1. It can be moved

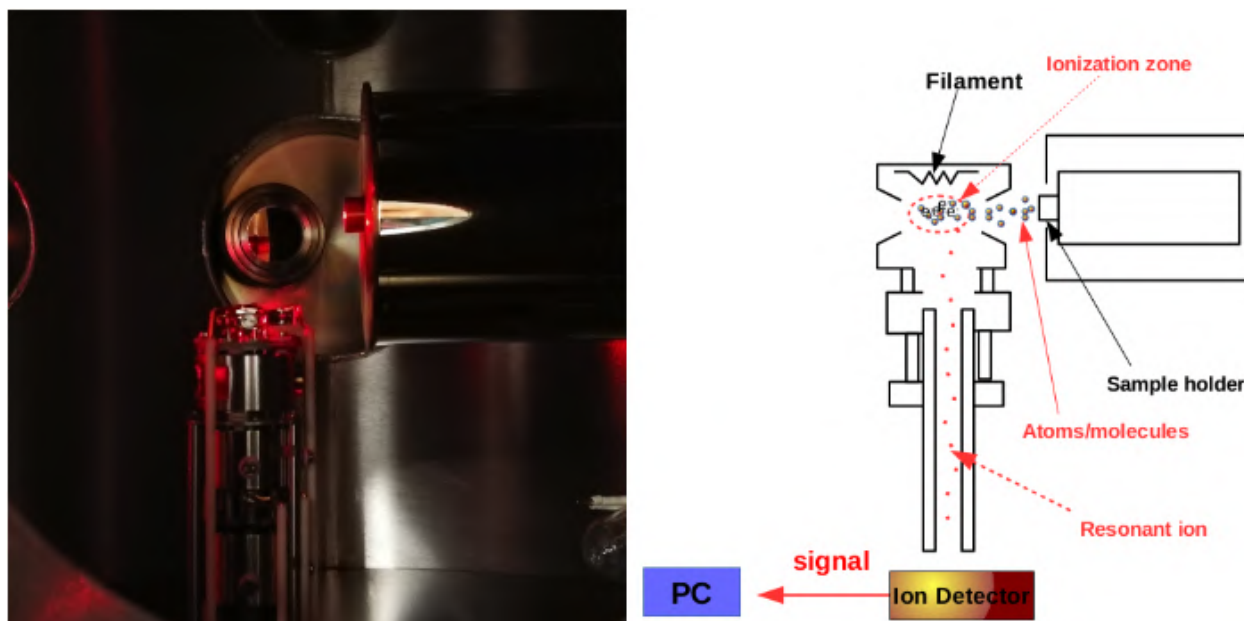


Figure 3.4 – At the left panel, an image of the QMS in front of the sample. At the right panel a sketch of the QMS. Credit: [12]

on the vertical (z axis). If the QMS is in front of the sample, it measures molecules during a TPD. If it is at the bottom position, it measures the residual gas in the principal chamber.

3.1.5 Fourier transform Infrared (FT-IR) spectrometer

The spectrometer used on VENUS is a VERTEX 70v Fourier transform Spectrometer (FTIR) which is used to monitor adsorbed/formed species *in situ*. This apparatus is a Michelson spectrometer. Detailed in the figure 3.5, this consists of mid infrared (MIR) source with a wide wavelengths range from 2.2 to $14.3\mu\text{m}$ is splitted by a beamsplitter in two beams. The two beams are reflected by mirrors and converted back to the beam splitter which reflects them or lets them pass over a new mirror. The beam is then directed onto the sample surface at an angle of $83 \pm 1^\circ$ and returned to the detector. When the two beams recombine, they have not necessarily traveled the same distance, which creates interference. By performing a Fourier transform on the signal detected with the detector, we can find the wavelength. The detector measures the absorbance, i.e. the difference between the empty laser signal (background) and the measured signal. Illustrated in figure 3.1, the spectrometer step angle allows to measure spectra during a beam deposition and during a TPD.

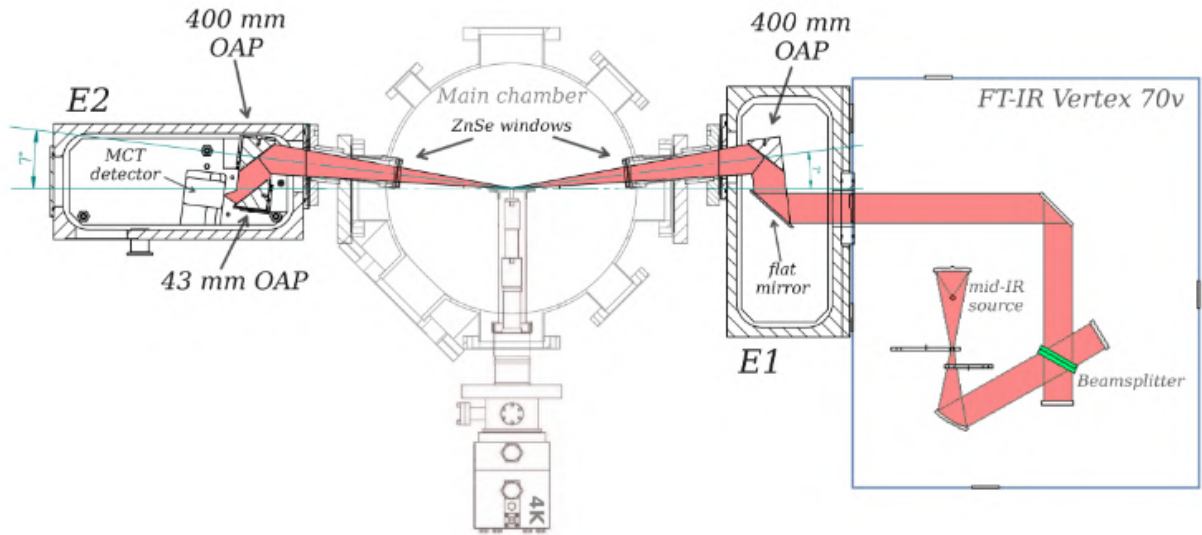


Figure 3.5 – Schematic view of the infrared system in VENUS. Credit: [17]

3.2 Experimental methods

3.2.1 Optimization of the beam flux

The first step when starting a series of experiments is to calibrate the beam fluxes. We will choose different flows for our beams that we will measure directly with the QMS and we will produce a saturation curve. The figure 3.6 is a saturation curve of the nitrogen. It shows the variation of the signal at the sample in function of the pressure (or flux) injected in the beam line. The curve has two trends, at small flux values the curve increases linearly, while at large flux values the curve converges to a maximum. At the transition of the two modes, represented by a red cross on the figure 3.6, we suppose that we deposit a monolayer² in 10min.

3.2.2 Temperature Programmed Desorption (TPD)

Temperature Programmed Desorption (TPD) consists in heating the surface with a linear ramp and to measure with the QMS what desorbs. The ramp is described at the equation 3.1:

$$T = T_0 + \beta t \quad (3.1)$$

where T is the temperature (in K) at a time t (in s), T_0 is the starting temperature (in K) and $\beta = \frac{dT}{dt}$ the temperature ramp (in $K s^{-1}$). In our set-up, the ramp is $\beta = 0.2 K s^{-1} = 12 K min^{-1}$. This choice of ramp allows to have an interesting signal/noise ratio while

2. A monolayer is when one species completely covers the surface of our sample. The thickness of the monolayer is one molecule. We calculate that a monolayer corresponds to $10^{15} mol/cm^2$.

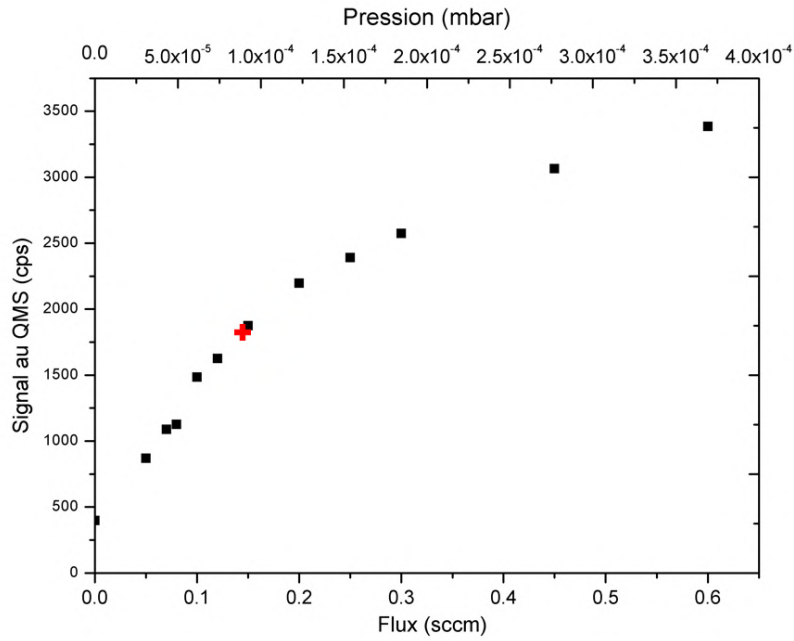


Figure 3.6 – N_2 beam flux as a function of source flux

having a rather short experiment time (approximately 24 minutes to make $10 \rightarrow 300K$). In the literature you can see other ramps for examples $2K \text{ min}^{-1}$ or $5K/\text{min}$ [19][20]. But using lower ramps allows detailed study of the sub-monolayer.

One explanation of TPD curves is a distribution of binding energy in a adatoms-surface system [21] [1]. Figure 3.7 illustrates the phenomenon. The chemical species accrete on the surface and diffuse. As it diffuses, it moves to the least energetic adsorption sites and therefore where the temperature is highest at the TPD curve (a panel in the figure 3.7). The more chemical species that accrete, the more adsorption sites on the surface are occupied, until none are available. This is called the monolayer (b panel of the figure 3.7). All the new chemical species will now be deposited on the monolayer. In the figure 3.7, only N_2 is deposited on the surface. So when we are in a multilayer, i.e. we deposit on top of the monolayer, all the adsorption sites are identical and therefore we have the same binding energy. This results in desorption at the same temperature of the TPD (c panel of the figure 3.7).

In our experiments, this is how we calculate the time it takes for a beam to cover our surface with a monolayer of molecules. We compare qualitatively different TPD curves with different deposition times. The one that has an almost identical rising edge to a multilayer without having the same shape is the TPD of the monolayer (see figure 3.8).

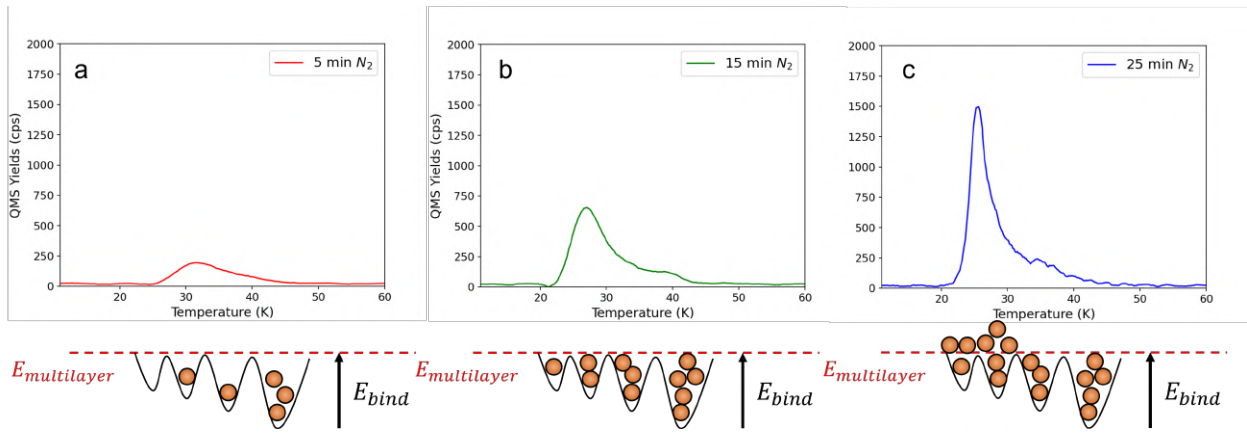


Figure 3.7 – TPD curve of N_2 after different deposition times (5, 15 and 25 minutes, respectively a, b and c panels). The diagrams below the curves represent the occupied sites. The particles fill the most energetic sites first.

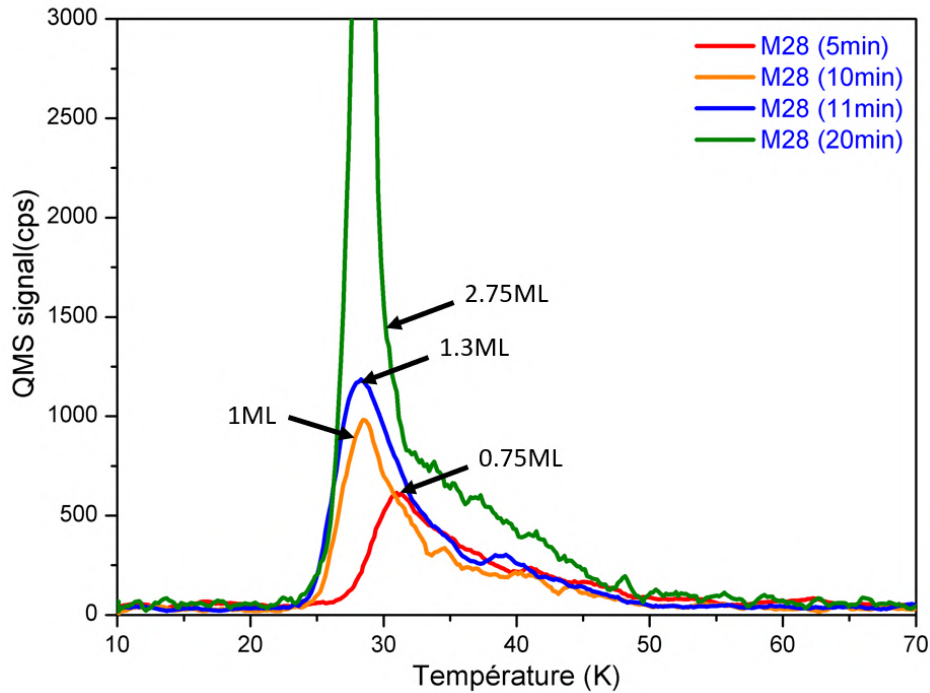


Figure 3.8 – TPD curves of mass 28 which represent de CO during different time of deposition (5, 10, 11, 20min). The curve in orange represent the monolayer.

3.2.3 Dissociation of H_2

To obtain atomic hydrogen is not in a gas bottle because it would instantly recombine with itself. However we want to experiment with atomic hydrogen. To do this, we will dissociate molecular hydrogen H_2 using a microwave source. The figure 3.9 shows a picture of dissociation of H_2 gas on the right beam of VENUS.

To calculate the H_2 dissociation rate, we measure the H_2 flux with or without dissociation at

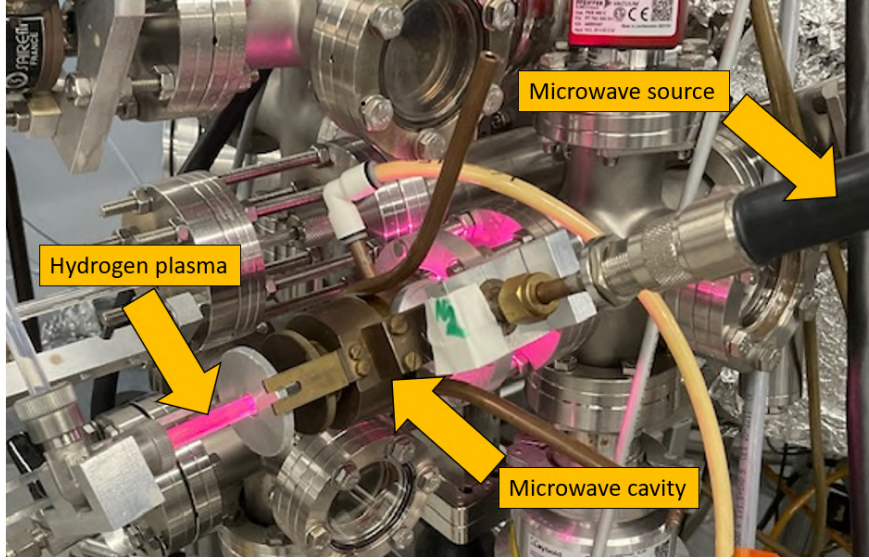


Figure 3.9 – Hydrogen plasma in the right beam of VENUS

the QMS. To constrain the dissociation rate we also measure the H_2 flux with the half-valve. The dissociation rate is then calculated:

$$\tau_{diss} = \frac{(N_{off} - H_2^{diff}) - (N_{on} - H_2^{diff})}{N_{off} - H_2^{diff}} \quad (3.2)$$

where N_{off} the value measure by the QMS without dissociation, N_{on} with dissociation and H_2^{diff} is define as

$$H_2^{diff} = \frac{N_{off}^{1/2} + N_{on}^{1/2}}{2}. \quad (3.3)$$

Where $N_i^{1/2}$ is the value measure by the QMS with the half-valve.

3.2.4 Cracking pattern

Presented in the subsection 3.1.4, the QMS detects the molecules after having ionized them. Electrons are pulled out of the molecules resulting in their ionization. However, the electron stripping by collision can fragment the molecule. These fragments are called Cracking Patterns. The ionization and collision fragmentation are different for each molecule. This depends on the geometry, angle of impact between two molecules or the electron, the energy of the ionizing electron. If we want to know the exact amount of molecules formed, we must take into account the cracking pattern. The signals at different masses can derive from the same molecules. For example, the figure 3.10 shows the TPD curves of six masses: 15, 28, 29, 30, 31 and 32. The signals of this masses have the same form and derive of the same molecule: the methanol (CH_3OH). Table 1 reports the cracking pattern of the molecules that will be studied in the experiments carried out.

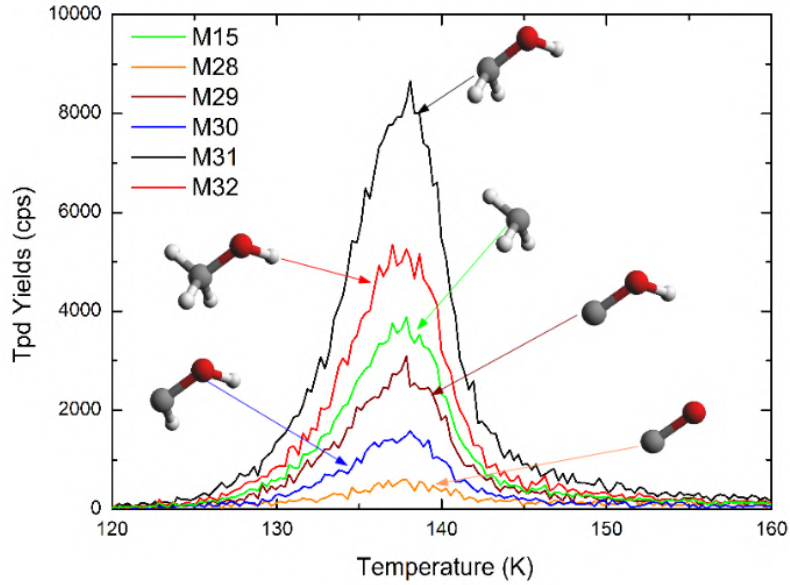


Figure 3.10 – TPD curves of masses 15, 28, 29, 30, 31 and 32. This experiment is a deposition of 1ML of methanol. All peaks have the same shape but not the same mass intensity. This represents the same molecule but which has been fragmented by QMS. Credit:[11]

Molecule	Peak 1	Peak 2	Peak 3	Peak 4
	Mass-%			
Dioxygen (O_2)	32-100	16-8.5		
Water (H_2O)	18-100	17-26	16-0.1	
Hydrogen peroxide (H_2O_2)	34-100	18-45	17-41	33-12
Carbon monoxide (CO)	28-100	29-2.5	12-2	
Carbon dioxide (CO_2)	44-100	28-8	16-4	12-4
Formaldehyde (H_2CO)	30-100	29-22	31-10	
Methanol (CH_3OH)	31-100	32-75	29-45	15-12

Table 1 – List of cracking pattern of molecules used in the experiments: O_2 , H_2O , H_2O_2 , CO , CO_2 , H_2CO and CH_3OH . The mass is indicated in blue and the intensity in red. The signals is normalized to the highest mass signal.

4 Prior experiment

4.1 Formation of water

4.1.1 The possible reaction

In the universe, water is very abundant especially in the solid phase. It is observed in different astrophysical environments: interstellar clouds, comets, satellites, planets [22]. In the gas

phase, the density of particles is very low, in the order of 1000 particles per cubic centimeter p/cm^3 in molecular clouds. The probability to have one interaction between two particles is very weak. It has been suggested that grain-surface reactions explain the observation. The simplest process of water formation is by hydrogenation of atomic oxygen:



These reactions don't have an activation barrier because it is radical-radical reaction. A second possible process to form water is the interaction of OH with H_2 :



But the reaction has an activation barrier of $2600K$ in the gas phase [23]. Alternative processes are proposed by Tielens and Hagen [24]:



Where the reaction 4.4 have no activation barrier [25], reaction 4.7 has an activation energy $\approx 2000K$ [26].

4.1.2 Co-deposition of O₂ and H

The formation of water is done by the hydrogenation of oxygen so two experiments must be done, $O + H$ and $O_2 + H$. Unfortunately, in this report the experiments with atomic oxygen will not be reported. Atomic oxygen O is obtained by dissociating molecular oxygen O_2 following the same procedure as described in section 3.2.3. However, the plasma was rarely stable or the dissociation rate was too low in our experiment. So the experiments with O were postponed to later in the year but that has been already studied by [27] and [28].

The co-deposition of $O_2 + H$ can create different products, OH , HO_2 , H_2O and H_2O_2 if we take into account the reactions 4.2 and 4.5 to 4.7. OH and HO_2 are radicals so the reaction time of H is too short to detect these species. Oba et al. (2009)[9] studied the co-deposition of O_2 and H and they showed that the abundance of H_2O and H_2O_2 depended on the O_2/H ratio and the temperature of substrate during the deposition. Oba et al. (2009)[9] show that the higher the O_2/H ratio is, the more H_2O_2 there is.

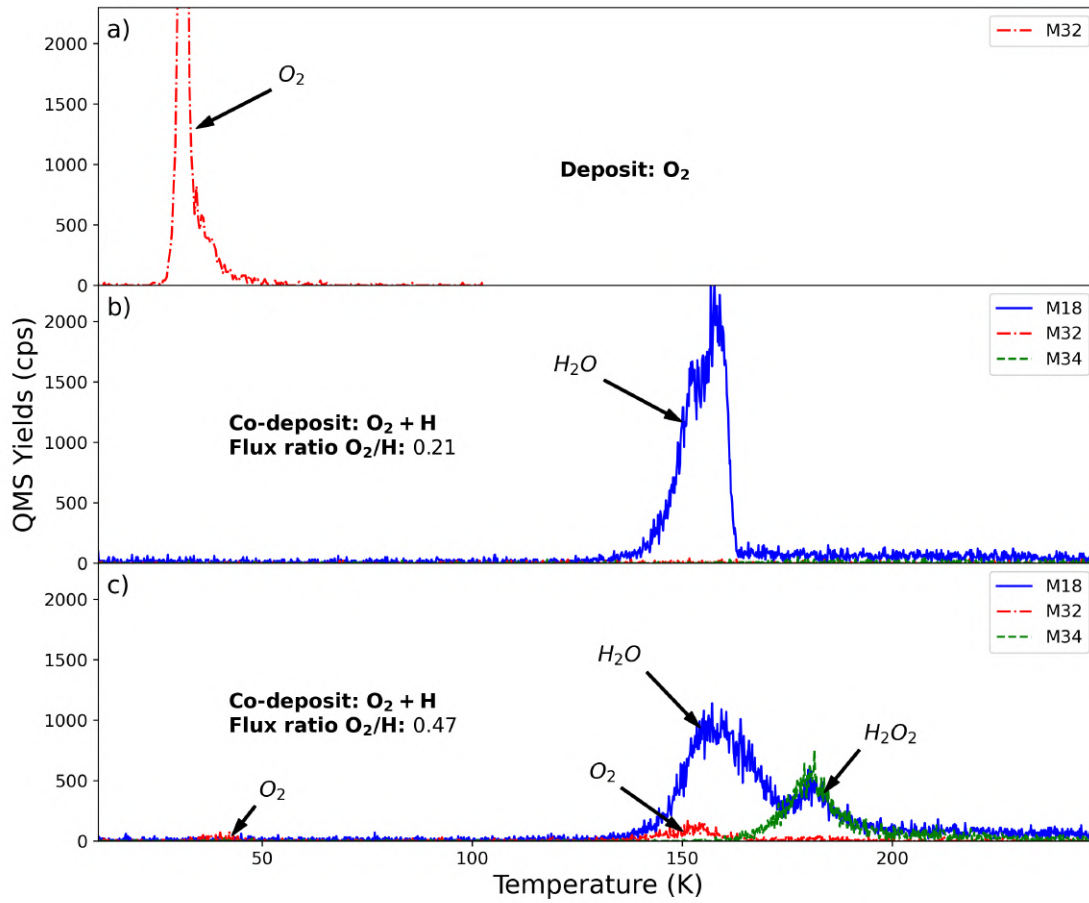


Figure 4.1 – TPD curve of products after three different experiments with same duration $60min$ and same surface temperature $10K$. a) TPD curve of mass 32 after deposition of O_2 . b) TPD curve of masses 18, 32 and 34 after co-deposition of O_2 and H with a flux ratio $O_2/H = 0.21$. c) Same as b) but with flux ratio $O_2/H = 0.47$.

We have redone this experiment which the results are represented in the figure 4.1 but in contrast to Oba et al.(2009)[9] I use Thermal Programmed Desorption (TPD) measured by the quadrupole mass spectrometer (QMS) and not the infrared spectrum. Are represented the TPD curves of three different experiments with well defined initial conditions, gold substrate, surface temperature at $10K$ and a deposition time of $60min$. The first experiment is a deposit of O_2 only. The top panel in figure 4.1 a) represent the Thermal Programmed Desorption (TPD) of this experiment. Oxygen has an atomic mass of 16, so the molecular oxygen O_2 has an atomic mass of $2 \times 16 = 32 uma$. That is why in this TPD, the mass 32 is measured and you can see the molecular oxygen desorb at a temperature around $T \sim 30K$. The central panel in figure 4.1 b) represents a TPD curve of masses 18, 32 and 34 where I have co-deposited O_2 and H with a flux ratio $O_2/H = 0.21$. The masses of water and oxygenated water are $m_{H_2O} = 18 uma$ and $m_{H_2O_2} = 34 uma$. The TPD curves show that

the H_2O is the only product at the end and all the molecular oxygen O_2 reacted. The flow of atomic hydrogen H was sufficiently important for the reaction 4.7 to be totally effective. But looking at the bottom panel in figure 4.1 c) where the flux ratio was $O_2/H = 0.47$. Three molecules were detected O_2 , H_2O and H_2O_2 . The detection of O_2 and H_2O_2 in the TPD shows that the hydrogenation was not sufficiently efficient. Moreover, O_2 desorbed together with water at $T \sim 152K$. This is due to the oxygen captured by the water during its formation and that could not react with the atomic hydrogen. The molecule H_2O_2 has a desorption peak at $T \sim 181K$ on the gold substrate. The mass 18 has the same trend as mass 34 which shows a cracking pattern (described at the section 3.2.4) of H_2O_2 . The abundance of H_2O_2 is almost equal to that of H_2O , so the O_2/H ratio influences the formation of water. We find the same results as Oba et al. (2009) [9].

Now for the temperature, when you increase the surface temperature, the hydrogenation is much less efficient because the desorption temperature of H_2 is $13K$. The hydrogen sticks to the surface and has a probability to leave it so it has less time to react with other chemical species. That explains why Oba et al. (2009)[9] find more H_2O_2 when they increase the temperature.

In molecular clouds, the abundance of H_2O is much higher than the abundance of H_2O_2 . It has been theoretically estimated that $H_2O/H_2O_2 > 30$ in the Orion molecular cloud core [29]. Moreover the observation of *NGC7538:IRS9* estimates $H_2O_2/H_2O < 0.5$ [30]. For the future experiments, I maximized the H_2O formation to correspond to the astrophysical condition so I placed myself in the condition of $O_2/H = 0.21$.

4.2 Formation of methanol

4.2.1 The possible reaction

The hydrogenation of the CO can form principally two molecules, formaldehyde H_2CO reaction 4.8 and at the end the methanol CH_3OH reaction 4.9.



where Hiraoka et al. (2002)[31] studied in particular the reactivity of $CO + H$ reaction 4.8 and Watanabe et al. (2004)[32] and Fush et al. (2009)[33] the reaction 4.9. But it has been shown that the chemical species formed by the hydrogenation of CO can be dehydrogenated [34]. That is represented in the reaction 4.10.



The possible reactions of CO hydrogenation are summarized in the figure 4.2 presented by Minissale et al. (2016)[35]. In this paper, they have shown that during the hydrogenation of CO, there are molecules that leave the surface due to the chemical desorption described in the section 2.1.2.

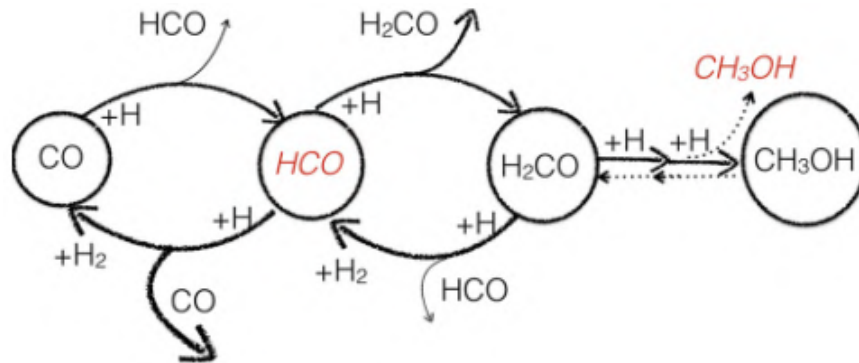


Figure 4.2 – Scheme of the CO–H chemistry [35]. The molecules in red are not detected in their experiments.

4.2.2 Co-deposition of CO and H

The goal of this internship is to study the formation of water in the presence of CO , i.e. in terms of experiment to make a co-deposit of $CO + O_2 + H$. However before doing this, we need to do some reference experiments. Previously in the section 4.1.2 I presented the $O_2 + H$ reference experiment in the central panel in the figure 4.1. Now we have to see the $CO + H$ experiment which is represented in figure 4.3. The experimental conditions are the same as $O_2 + H$ i.e. a 60min co-deposition with a surface temperature at 10K. Moreover the flux ratio $CO/H = 0.5$.

On the figure 4.3 , three chemical species are highlighted with the TPD curve:

- CO : represented with the masses 28 and 29. The carbon having an atomic mass of $C = 12\text{ uma}$ and oxygen $O = 16\text{ uma}$. The main mass of carbon monoxide CO is 28. However the bottle of CO is not totally pure, we can find an isotope of carbon $C = 13\text{ uma}$ so the measure of the mass 29 is important.
- H_2CO : Formaldehyde has an atomic weight of $H_2CO = 30\text{ uma}$. Moreover it is also necessary to take into account the cracking pattern that our QMS is able to measure, so the mass 29.
- CH_3OH : Methanol has a very long list of cracking patterns which is illustrated in the figure...(figure section cracking pattern) . With the quantities we form they are not all detectable. In this experiment methanol is only detected by masses 29, 31 and 32. Its atomic mass is $CH_3OH = 32\text{ uma}$.

We can notice that on this experiment, the CO has almost not reacted with the hydrogen. The figure 4.4 is a TPD curve of mass 28, and zooms in the desorption of CO . We notice

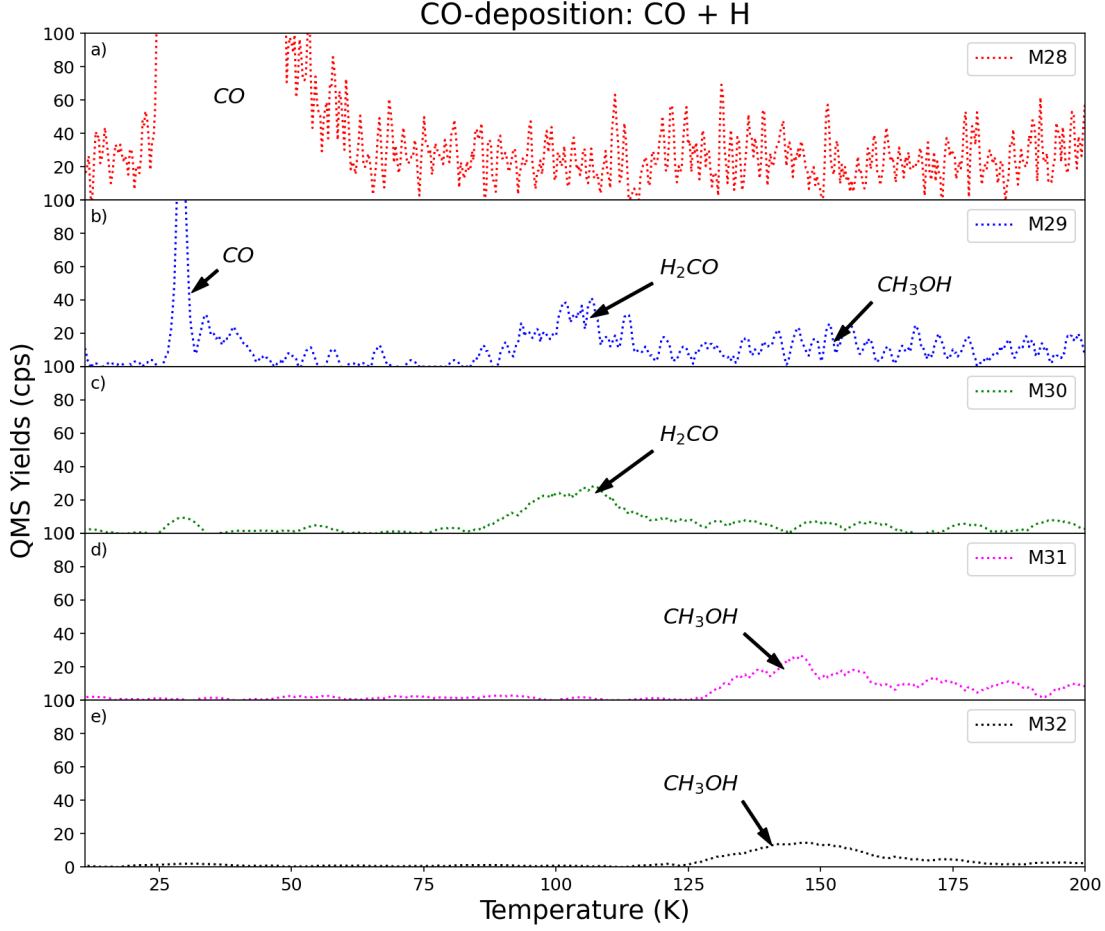


Figure 4.3 – TPD curves of masses 28, 29, 30, 31 and 32 for a experiment of co-deposition of CO and H during $60min$ with a surface temperature at $10K$ on a gold substrate.

that the maximum measured is $\sim 14000cps$ while H_2CO and CH_3OH have their maximum around $\sim 40cps$. In terms of quantity, we find 2.68% of formaldehyde and 4.04% of methanol. 80.98% of CO did not react. In comparison with the O_2+H experiment if we see the figure 4.1 at the middle panel, 100% of the O_2 reacted.

$$f(x) = ae^{-t/\tau} + b \quad (4.11)$$

To explain that, see the figure 4.5 which represents the decay of the O_2 and CO monolayer by the H-atoms irradiation. The figure 4.5a is the experiment where I deposit 1 ML of O_2 and irradiate by H-atoms during different times. At each different exposure time, I made a TPD and calculate the area of the TPD curve of mass 32 to know the amount of O_2 that did not react. The figure 4.5b is a deposition of 1 ML of CO irradiated by H-atoms during 40min. One IR spectrum is taken every 2min.³ The decay of the monolayer can be fitted

3. Taking TPDs at different times of exposure to H-atoms is very time consuming because a monolayer of

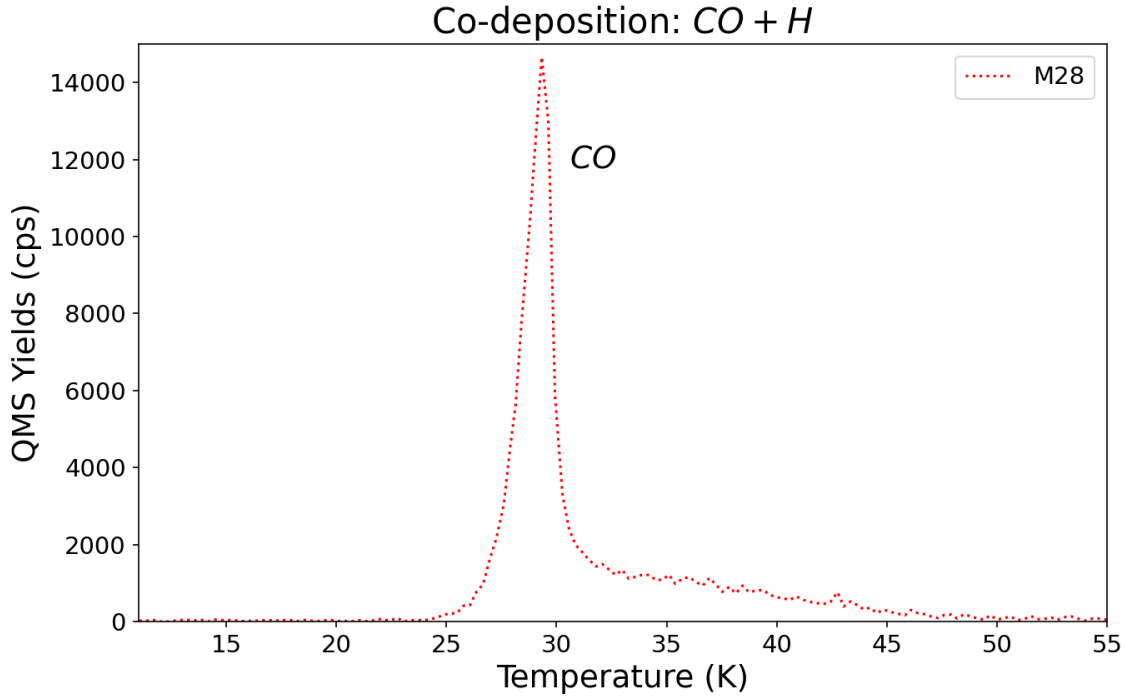


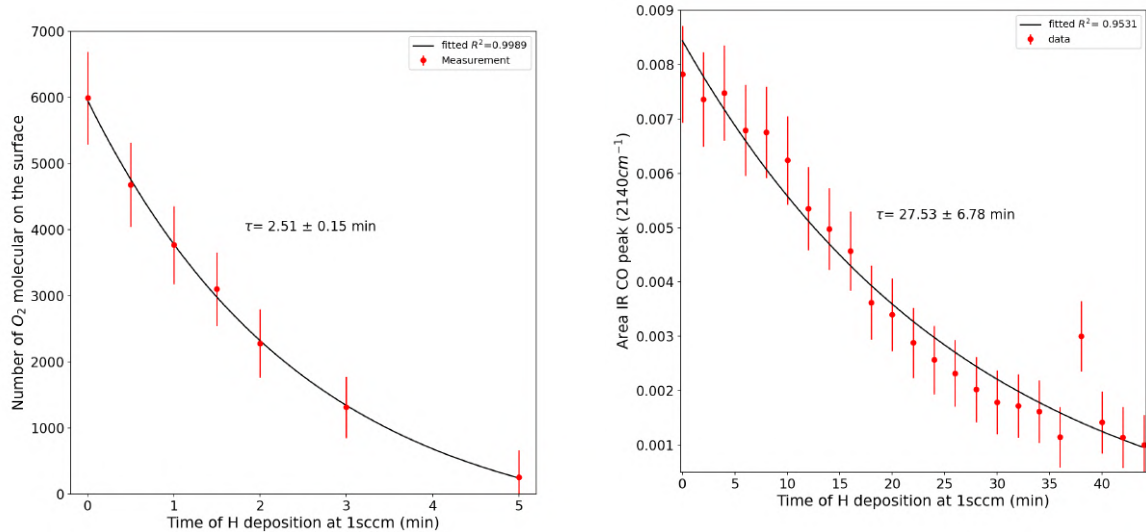
Figure 4.4 – Zoom on the TPD curve of the figure 4.3 from mass 28 on the CO peak.

by a decreasing exponential described in equation 4.11. Thus we can calculate the mean lifetime τ of the monolayer which gives us a good approximation of the reaction time of $O_2 + H$ and $CO + H$. The mean life time for O_2 is $\tau_{O_2} = 2.51 \pm 0.15 \text{ min}$ whereas for CO it is $\tau_{CO} = 27.53 \pm 6.78 \text{ min}$. The difference is huge and it can explain why the CO did not react. The time for two hydrogen atoms to form molecular hydrogen t_{H_2} is much less than the reaction time of $CO + H$: $t_{H_2} \ll \tau_{CO}$. This can be explained by the presence of a barrier for the reaction $CO + H$ and not for $H + H$ because they are two radicals. So when we codeposit CO and H , the H will react with each other without having time to react with a CO .

4.3 The gas phase

During our experiments, we can see losses of chemical species. To see that, we compare an experiment where we have deposited a chemical species (for example here CO or O_2) with the same experimental conditions. The figure 4.6 shows the PDT curve of mass 28 (which is represent the CO stick on the surface) for three experiments. The black solid curve represent a deposition of CO , the red dashed curve is the co-deposition of CO and H . The last blue

the chemical species must be deposited each time. Infrared spectrum is preferred for this kind of experiment because one can make spectra at the same time as the deposition. However some molecules are not detectable in the infrared like O_2 because it is a symmetrical molecule which implies that it has no dipole moment so no rotational or vibrational spectroscopy.



(a) Area of TPD curve of mass 32. The experiment is 1ML of O_2 deposited on the surface at 10K and irradiated by H atoms during 30s, 60s, 90s, 120s, 180s and 300s.

(b) Area of IR peak of CO ($\sim 2140cm^{-1}$). The experiment is 1ML of CO deposited on the surface at 10K and irradiated by H atoms during 40min. During the deposition, an IR spectrum is acquired every 2 min.

Figure 4.5 – O_2 and CO monolayer decay by H-atom irradiation

dotted curve is the $CO + O_2 + H$ experiment but it will interest us later. The shape of the TPD curve is similar between the CO and $CO + H$ experiment. However, we notice that the maximum is more for $CO + H$ and the area is less important. This shows that CO has reacted with hydrogen on the surface as seen in the previous section. However we do not find all the CO deposited. The figure 4.7 a) represent the distribution of CO deposited between the products, the CO that has not reacted and a lost part. The lost part represents what was not detected by the QMS at the end of the experiment, i.e. what returned to the gas phase. The chemical phenomenon is called direct chemical desorption [13] which is described in the section 2.1.2. It is assumed that when two chemical species react with each other on the surface, there is a probability that the excess energy due to the reaction will result in desorption of the newly created molecule. This phenomenon is also seen by Minissale et al. (2016)[35] with a co-deposition of $CO + H$.

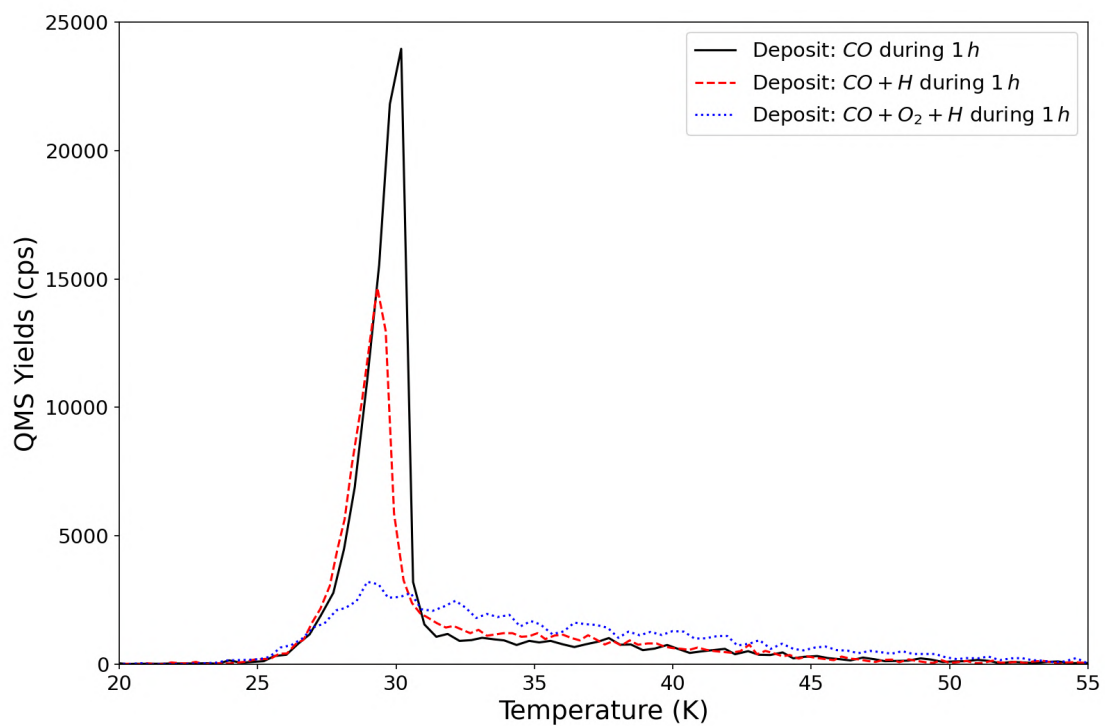


Figure 4.6 – TPD curves of three experiments: the solid black curve is a deposition of CO , the dashed red curve is a codeposition of CO and H and the dotted blue curve a codeposition of CO , O_2 and H .

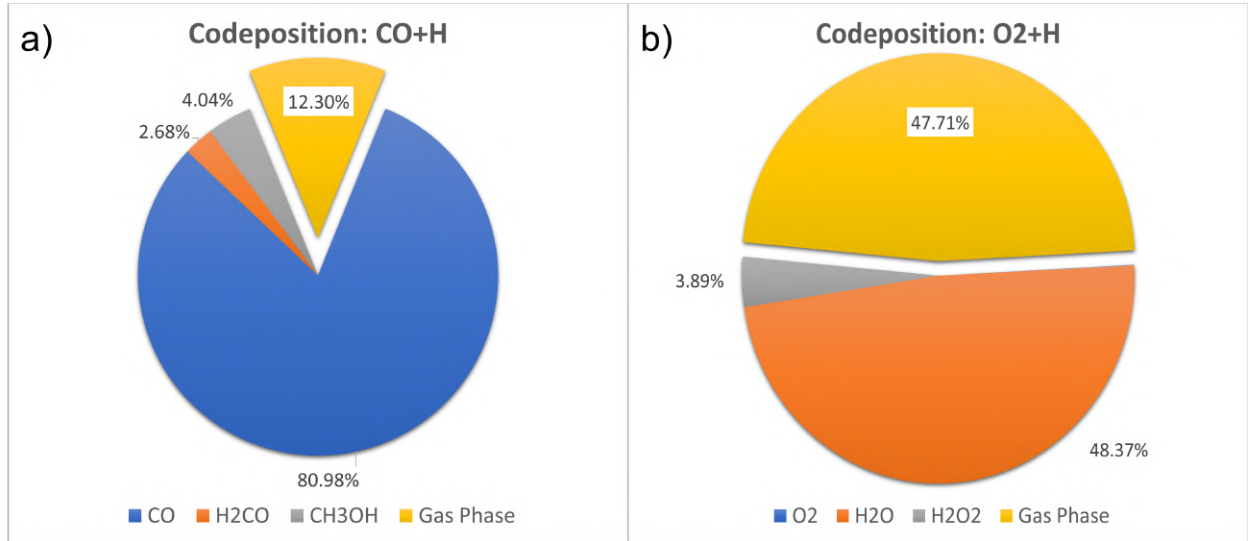


Figure 4.7 – Pie charts of a distribution of products created by hydrogenation experiments. At the left panel, it is a codeposition of CO and H and at the right panel a codeposition of O_2 and H . The error is around 2-3%.

We remark that for the co-deposition $CO + H$, we have 12.3% of the CO was ejected in the gas. In the figure 4.7 b) we have the same diagram but for the experiment $O_2 + H$ and we can see that 47.71% return in the gas phase, it is very huge. The molecules ejected in the gas are calculated with the equation 4.12 for CO and equation 4.13 for O_2 .

$$L_{CO} = 1 - \frac{N^{CO} + N^{H_2CO} + N^{CH_3OH}}{N_{ref}^{CO}} \quad (4.12)$$

$$L_{O_2} = 1 - \frac{N^{O_2} + N^{H_2O}/2 + N^{H_2O_2}}{N_{ref}^{O_2}} \quad (4.13)$$

where N^i is the number of molecules detected by the QMS during the TPD such as $N^i = \int_{T_a}^{T_b} Mass(i)$ where i is the molecule. N_{ref}^{CO} is the total number of molecules of CO deposited on the surface by beam. Now we can study the subject of this internship, i.e. the formation of water in the presence of CO on interstellar dust grains.

5 Formation of water in presence of CO

In the previous section, we have seen which condition we had to respect to overhydrogenate our oxygen. In addition, we have studied the hydrogenation of carbon monoxide and molecular oxygen. The question now is: what would happen if we formed water in the presence of CO ? That is to say, does a $CO + O_2 + H$ co-deposition experiment. I use exactly the same conditions as the previous experiments: gold substrate, surface temperature at $T = 10K$, irradiation of the surface by CO , O_2 and H during 60min, the ratio of fluxes are $O_2/H = 0.21$

and $CO/H = 0.5$. I deposit 6 ML of O_2 and 8.37 ML of CO.

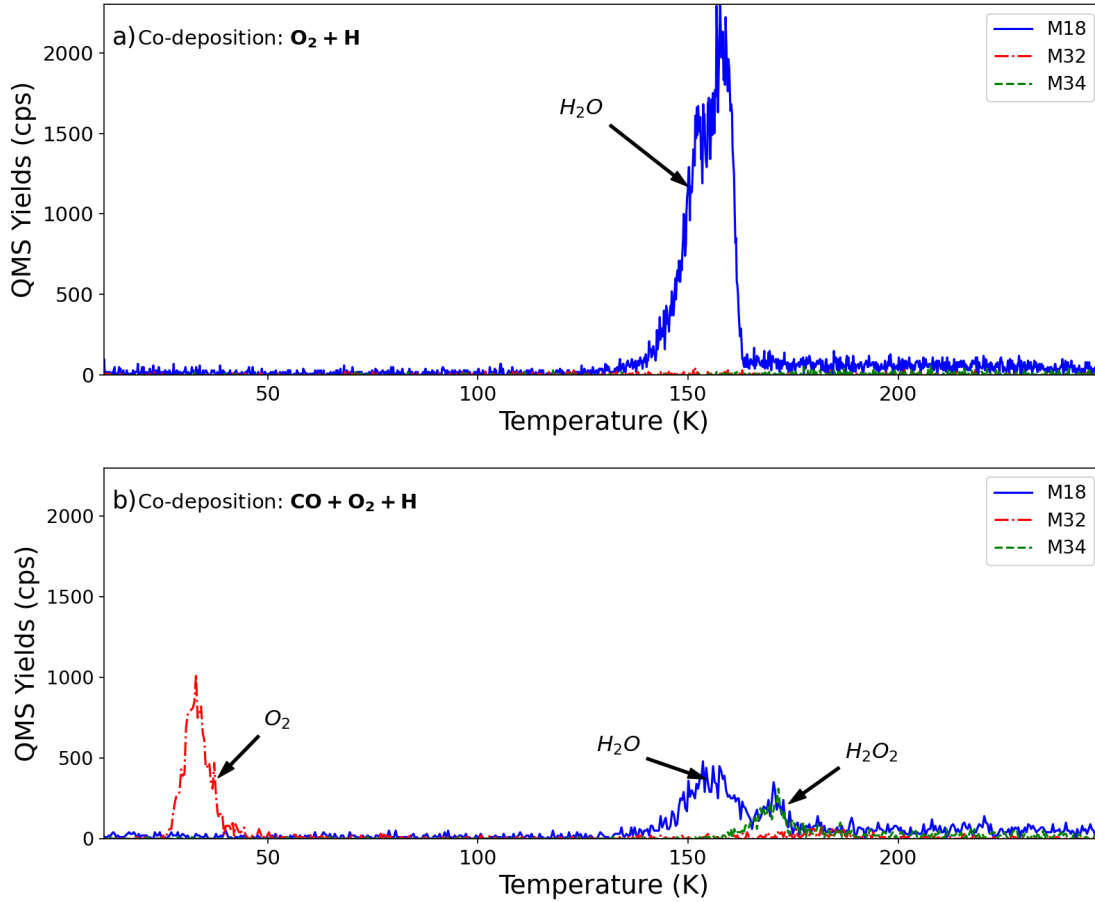


Figure 5.1 – TPD curve of mass 18, 32, 34 of two experiments: a) co-deposition of 6 ML of O_2 and H , b) co-deposition of 8.37 ML of CO and 6 ML of O_2 and H .

Figure 5.1 shows two TPD curves of masses 18, 32 and 34 *amu* where at the top panel is the co-deposition $O_2 + H$ and at the bottom panel the co-deposition $CO + O_2 + H$. We can see that for the $CO + O_2 + H$ co-deposition experiment (bottom panel figure 5.1), there is a large signal from mass 32 around 30K. It is molecular oxygen O_2 that has not reacted. In addition, we notice a signal from mass 18 and 34 at temperature of about 168K which is H_2O_2 . The mass 18 peak at 150K is the water H_2O . We notice that the CO prevents the O_2 and H_2O_2 from reacting with the atomic hydrogen, which leads to a decrease of the water formed. Quantitatively, if we look at the figure 5.2 b) in the right panel, only 13.28% of the O_2 deposited on the surface has produced H_2O . Therefore, we have 34.35% less water than with the $O_2 + H$ experiment. 25% of the O_2 did not react and we have 23.25% of H_2O_2 compared to 3% for the $O_2 + H$ experiment. We can notice the part of O_2 which returns in gas phase is less important but remains huge, 37.97%.

For the CO , it is more extraordinary. The figure 5.2 a) at the left panel shows the distribution

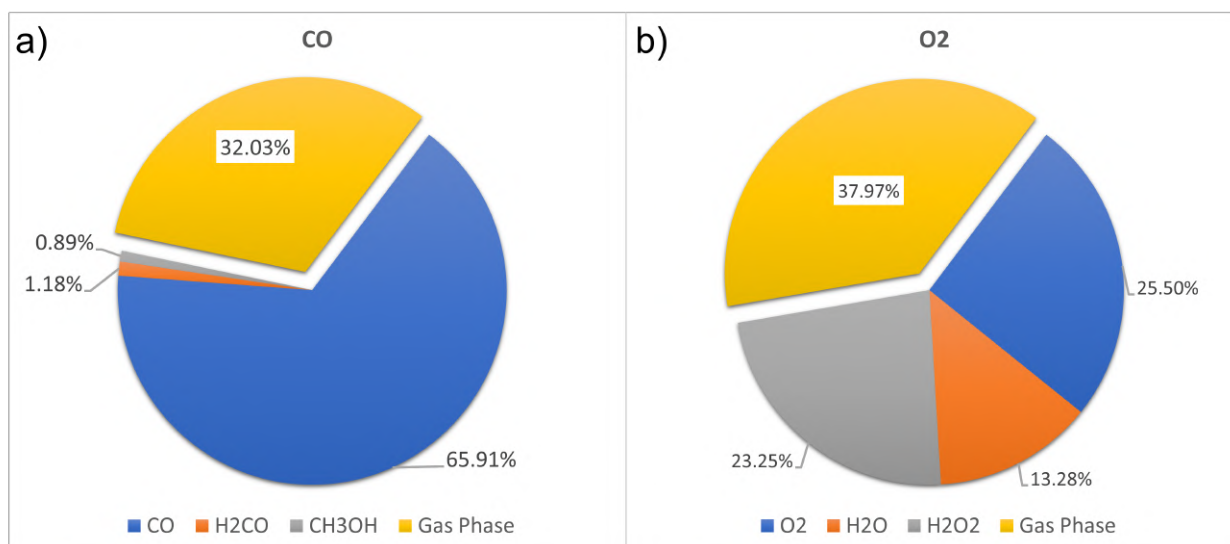


Figure 5.2 – Pie charts of the distribution of products created by the hydrogenation of CO in the left panel and the hydrogenation of O_2 in the right panel for a codeposition of CO , O_2 and H . The error is around 2-3%.

of product created by hydrogenation of the CO . 65.91% of the CO deposited on the surface did not react, it is less compared 80.98% of the experiment $CO + H$ (figure 4.7 in the left panel). But the CO did not react more, only 0.89% of methanol CH_3OH and 1.18% of H_2CO were found. It is on the side of the ejected CO that we must look. It has increased by 19.73% compared to $CO + H$. This gives us 32.03% of CO that is returned to the gas phase. This is curious because in this experiment I am co-depositing $CO + O_2 + H$. The initial quantity of hydrogen atoms remains the same, but here we have 2 reactants, so less possibility for each product from each hydrogenation reaction. This implies that the amount of direct chemical desorption should be less and thus less chemical species returning to the gas phase. So why does the amount of CO ejected from the surface increase?

The figure 5.3 confirms that less methanol and formaldehyde are formed. The figure 5.3 shows the TPD curves for masses 28, 29, 30, 31 and 32 respectively. The red dashed curve corresponds to the $CO + H$ experiment and the blue solid curve to the $CO + O_2 + H$ experiment. We notice that for masses 29 and 30 at 110K, which represent H_2CO , there is less signal and for CH_3OH at 130K with the masses 31, 32 and 29, the signal is also less important⁴.

Another way to confirm this loss is to look at the shape of the CO desorption and compare it to other experiments. The figure 4.6 shows a TPD curve of mass 28, representing the CO desorption peak. Three experiments are represented: solid dark curve for a deposition of CO during 60min at 10K, the red dotted curve for the experiment of co-deposition $CO + H$

4. On the TPD curve of mass 32, for the $CO + O_2 + H$ experiment, we see a signal at about 178K. This is due to the dismutation of H_2O_2 during water ice desorption: $2H_2O_2 \rightarrow 2H_2O + O_2$. The signal corresponds to the molecule O_2 . One can particularly find this phenomenon on comets. [36]

with same conditions, and the dotted blue curve for the experiment $CO + O_2 + H$. This last curve, the dotted blue, does not have a large multilayer peak. However the value in the tail is higher. In this experiment water is formed. Since the binding energy of water is higher than that of gold, so the CO molecules interacting with water will desorb at higher temperatures [37]. The blue dotted curve appears to have a smaller area than the other two curves.

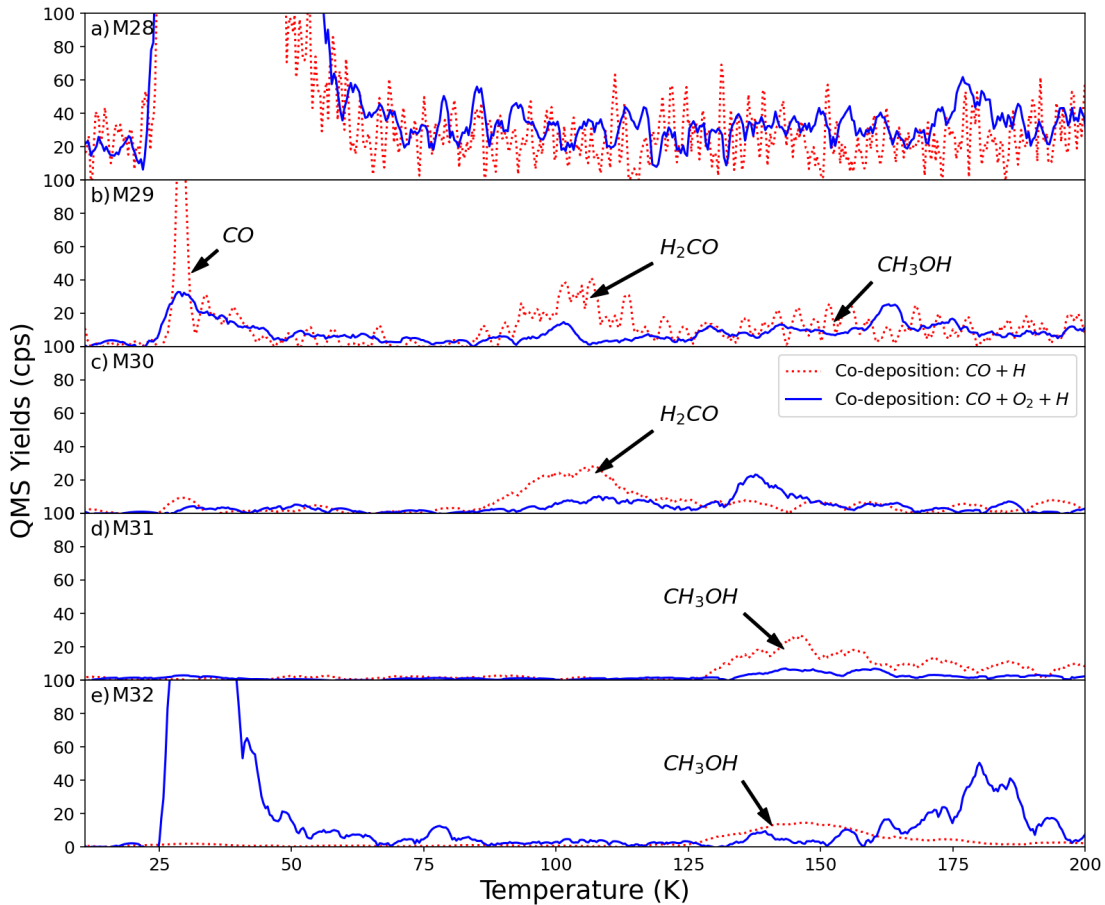


Figure 5.3 – TPD curves of masses 28, 29, 30, 31 and 32 for a experiment of co-deposition of CO , O_2 and H during $60min$ with a surface temperature at $10K$ on a gold substrate.

Next, we wanted to study the impact of surface temperature on CO and O_2 losses. Figure 5.4 shows a bar chart where the bins represent the surface temperature during deposition ($8.6K$, $10K$, $15K$, $20K$ and $25K$). The blue bar represents the CO ejected into the gas and the orange bar represents the O_2 . First of all, if we look at $25K$ we notice that 74% of the CO is ejected during the experiment. The temperature is very close to the desorption temperature of CO , so the CO has a non-zero probability of desorbing from the surface. For the other temperature, the percentage of CO and O_2 that are ejected in the gas remains almost the same except at $15K$ for the CO . We can notice an increase around 15%. It is

possible another effect may have been added, for example that the stickiness coefficient is less effective. But this is a hypothesis and it would be necessary to do another experiment to confirm it.

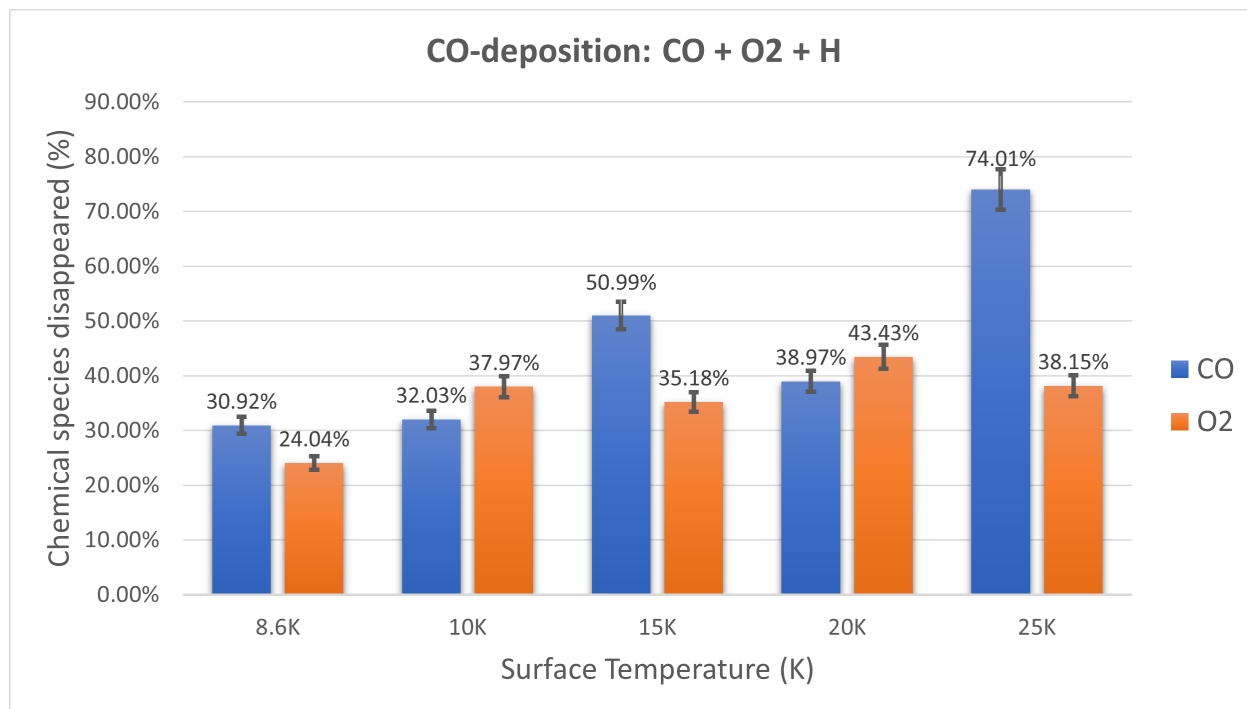


Figure 5.4 – Bar chart representing the loss of CO and O_2 in different surface temperatures (8.6K, 10K, 15K, 20K and 25K) in codeposition of CO , O_2 and H .

6 Indirect chemical desorption

The previous section showed that there were chemical species ejected from the surface that could not be explained by the chemical desorption described by Dulieu et al. (2013)[13]. This chemical desorption is described in the diagram in Figure3 which is renamed "*direct chemical desorption*".

In this report, I will introduce a new chemical desorption name "*indirect chemical desorption*". This is the same principle as direct chemical desorption but instead of the energy ejecting the molecule from the surface, it is the neighboring molecule that is ejected. It is assumed that the $OH + H$ reaction is responsible for this effect in our experiments. Indeed the reaction is exothermic with an enthalpy of reaction $\Delta_r H^0 = 492 \text{ kJ/mol}$. In comparison the reaction $CO + H$ has an enthalpy of formation $\Delta_r H^0 = 62 \text{ kJ/mol}$, $H_2CO + H$ has $\Delta_r H^0 = 301 \text{ kJ/mol}$ or the reaction $HO_2 + H$ has $\Delta_r H^0 = 361 \text{ kJ/mol}$. The figure 6.2 is a sketch of the indirect chemical desorption.

To illustrate the indirect chemical desorption, the molecule N_2 would be more appropriate. The binding energy is similar to CO but it does not react with H . If we detect N_2 losses in our TPD, we are sure that it is from of the indirect chemical desorption. Two experiments

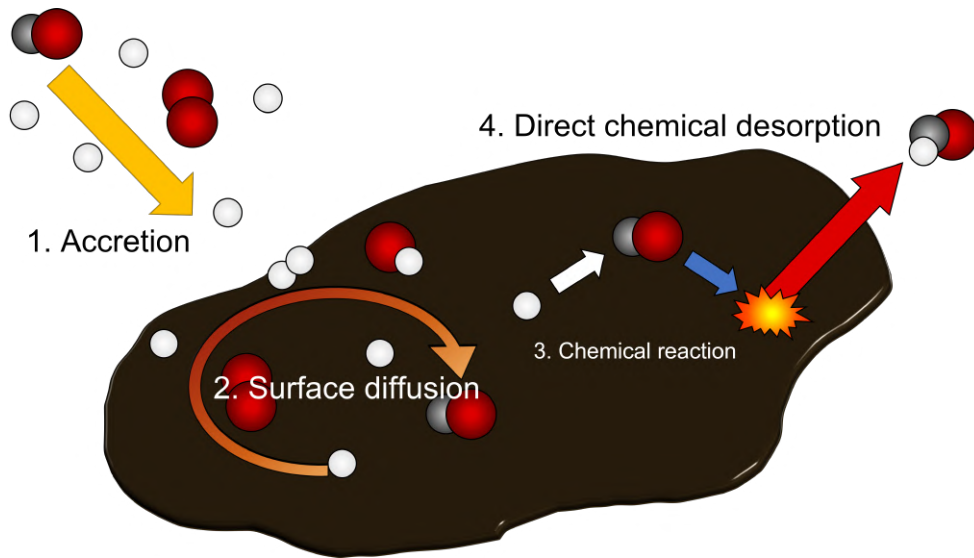


Figure 6.1 – Sketch of the direct chemical desorption process. Chemical species from the gas accrete on the dust grain. The species diffuses and reacts with another species on the surface. The excess energy due to the reaction ejects the newly formed species into the gas phase.

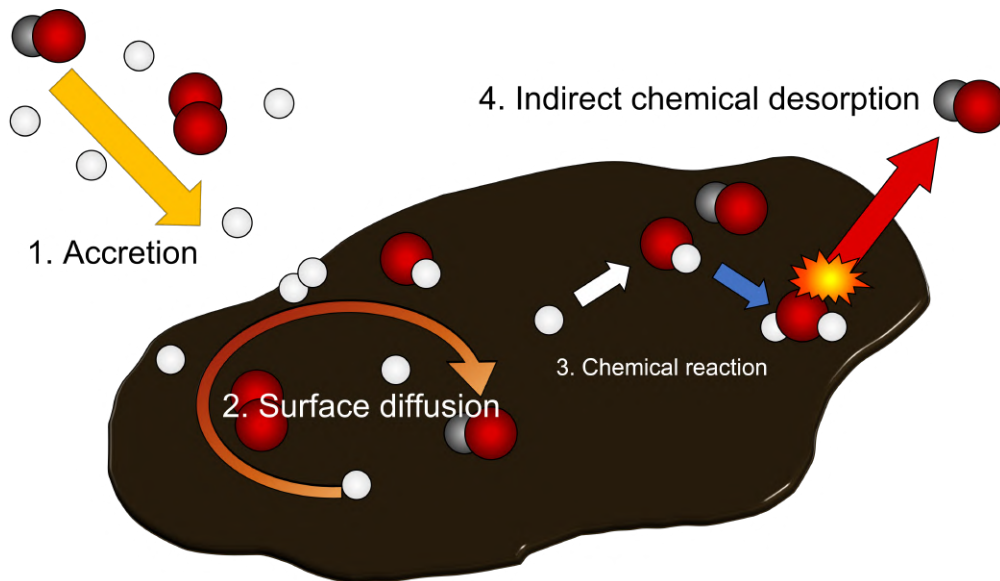


Figure 6.2 – Sketch of the indirect chemical desorption process. The chemical species of the gas accrete on the dust grain. The species diffuses and reacts with another species on the surface. The excess energy due to the $OH + H$ reaction diffuses into the neighboring species which is ejected into the gas phase.

were performed to codeposit N_2 , O_2 and H for 60 min at a surface temperature of 10K with the same flux ratio $N_2/H \approx 0.3$. Losses were detected during the TPD of 18% to 60% respectively. This gives us around $\sim 40 \pm 20\%$. The uncertainty is very large and the problem comes from the calculation of the total number of N_2 deposited on the surface. The figure 6.3 illustrates the problem very well. It shows the TPD curves of N_2 for three experiments: the black solid line is the depositions of N_2 during 20min multiplied by three to correspond to 60min of experiment, the red dashed line is a co-deposition of N_2 and H during 60min and the blue dotted line is a codeposition of N_2 , O_2 and H during 60min. The surface temperature for the three experiments is 10K. By multiplying the TPD 20min curve by three, the desorption tail is completely overestimated (from 28K to 50K). This implies that when calculating the area under the curve, we end up with a totally overestimated surface. This 20min N_2 deposition experiment allows us to estimate the number of N_2 deposited on the surface. Thus, when we calculate the number of N_2 that are returned to the gas phase, we end up with an overestimation of the latter. Normally the TPD curve for 60min of N_2 deposition at 10K looks like the TPD curve for CO with the same condition (figure 4.6, the solid dark curve).

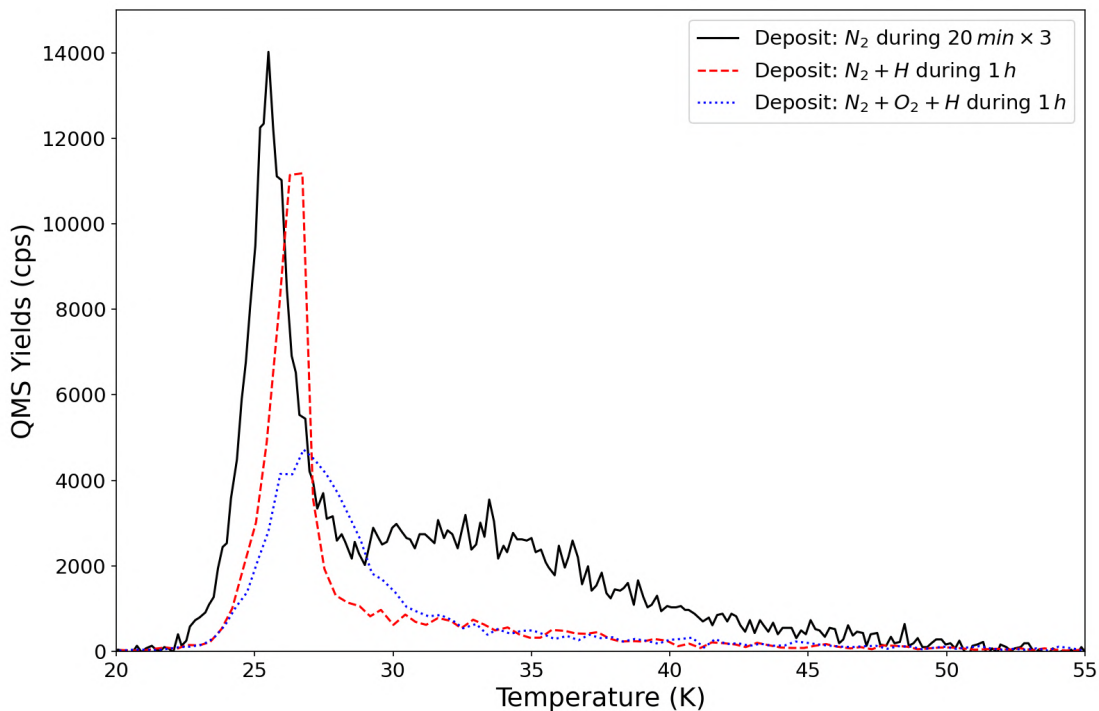


Figure 6.3 – TPD curves of the mass 28 which represent the N_2 for three different experiments: the solid black line is a deposition of N_2 during 20min where the result is multiplying by three to correspond at 60min of deposition, the dashed red line is a deposition of N_2 and H during 60min and the dotted blue line is a codeposition of N_2 , O_2 and H during 60min.

7 Conclusion

To conclude, after a long realization of experiments and preliminary analysis of the obtained results, we were able to identify a new type of chemical desorption that we named indirect chemical desorption. Induced for the formation of $OH+H$ it would be the cause of an ejection of the surface of N_2 , O_2 and CO of the order of 30% to 50%. However some experiments are missing to confirm this new chemical desorption and its real impact.

The next tracks of work during the thesis are:

- to redo codeposition experiments of N_2 , O_2 and H of 30min with good reference to illustrate the phenomenon of chemical desorption.
- replace N_2 by other chemical species like Ar , Ne , CO_2 , CH_3OH , ... where binding energy, mass and degree of freedom are different to see the impact on the indirect chemical desorption.
- To look at the influence of the flux by changing the ratio CO/H , N_2/H , ... on the indirect chemical desorption.
- Set up a physical model of indirect chemical desorption and compare with experiments.

References

- [1] L. Amiaud, J. H. Fillion, S. Baouche, F. Dulieu, A. Momeni, and J. L. Lemaire. Interaction of D_2 with H_2O amorphous ice studied by temperature-programed desorption experiments. , 124(9):094702–094702, March 2006.
- [2] Bruce T. Draine. *Physics of the Interstellar and Intergalactic Medium*. 2011.
- [3] David Hollenbach and E E Salpeter. Surface recombination of hydrogen molecules. *The Astrophysical Journal*, 163:155–164, 1971.
- [4] A C Adwin Boogert, Perry A Gerakines, and Douglas C B Whittet. Observations of the icy universe. *ARAA*, 53, 2015.
- [5] Edwin A. Bergin and Mario Tafalla. Cold Dark Clouds: The Initial Conditions for Star Formation. , 45(1):339–396, September 2007.
- [6] A. Bacmann, V. Taquet, A. Faure, C. Kahane, and C. Ceccarelli. Detection of complex organic molecules in a prestellar core: a new challenge for astrochemical models. , 541:L12, May 2012.
- [7] Catherine Walsh, Ryan A. Loomis, Karin I. Öberg, Mihkel Kama, Merel L. R. van 't Hoff, Tom J. Millar, Yuri Aikawa, Eric Herbst, Susanna L. Widicus Weaver, and Hideko Nomura. First Detection of Gas-phase Methanol in a Protoplanetary Disk. , 823(1):L10, May 2016.
- [8] Anna Punanova, Paola Caselli, Siyi Feng, Ana Chacón-Tanarro, Cecilia Ceccarelli, Roberto Neri, Francesco Fontani, Izaskun Jiménez-Serra, Charlotte Vastel, Luca Bizzocchi, Andy Pon, Anton I. Vasyunin, Silvia Spezzano, Pierre Hily-Blant, Leonardo Testi, Serena Viti, Satoshi Yamamoto, Felipe Alves, Rafael Bachiller, Nadia Balucani, Eleonora Bianchi, Sandrine Bottinelli, Emmanuel Caux, Rumpa Choudhury, Claudio Codella, François Dulieu, Cécile Favre, Jonathan Holdship, Ali Jaber Al-Edhari, Claudine Kahane, Jake Laas, Bertrand LeFloch, Ana López-Sepulcre, Juan Ospina-Zamudio, Yoko Oya, Jaime E. Pineda, Linda Podio, Davide Quenard, Albert Rimola, Nami Sakai, Ian R. Sims, Vianney Taquet, Patrice Theulé, and Piero Ugliengo. Seeds of Life in Space (SOLIS). III. Zooming Into the Methanol Peak of the Prestellar Core L1544. , 855(2):112, March 2018.
- [9] Y Oba, N Miyauchi, H Hidaka, T Chigai, N Watanabe, and A Kouchi. Formation of compact amorphous H_2O ice by codeposition of hydrogen atoms with oxygen molecules on grain surfaces. *The Astrophysical Journal*, 701:464–470, 2009.
- [10] A.G.G.M. Tielens. *Molecular Astrophysics*. Cambridge EBA Collection. Cambridge University Press, 2021.

- [11] Marco Minissale. *Physics and chemistry on the surface of interstellar dust grains : the effect of O-atom diffusion and chemical desorption on the H-C-N-O reaction network*. PhD thesis.
- [12] T. Nguyen. *Experimental study of desorption and reactivity of nitrogen bearing species on interstellar dust grains Experimental study of desorption and reactivity of nitrogen bearing species on interstellar dust grains A DISSERTATION PRESENTED*. PhD thesis, 2018.
- [13] François Dulieu, Emanuele Congiu, Jennifer Noble, Saoud Baouche, Henda Chaabouni, Audrey Moudens, Marco Minissale, and Stéphanie Cazaux. How micron-sized dust particles determine the chemistry of our Universe. *Scientific Reports*, 3:1338, February 2013.
- [14] David W. Savage, Gianni Astarita, and Shriram Joshi. Chemical absorption and desorption of carbon dioxide from hot carbonate solutions. *Chemical Engineering Science*, 35(7):1513–1522, 1980.
- [15] Valentine Wakelam, Emeric Bron, Stephanie Cazaux, Francois Dulieu, Cécile Gry, Pierre Guillard, Emilie Habart, Liv Hornekær, Sabine Morisset, Gunnar Nyman, Valerio Pirronello, Stephen D. Price, Valeska Valdivia, Gianfranco Vidali, and Naoki Watanabe. H₂ formation on interstellar dust grains: The viewpoints of theory, experiments, models and observations. *Molecular Astrophysics*, 9:1–36, 2017.
- [16] M. Minissale, E. Congiu, and F. Dulieu. Oxygen diffusion and reactivity at low temperature on bare amorphous olivine-type silicate. , 140(7):074705, February 2014.
- [17] Emanuele Congiu, Abdellahi Sow, Thanh Nguyen, Saoud Baouche, Francois Dulieu, E Congiu, A Sow, T Nguyen, " S Baouche, and F Dulieu. A new multi-beam apparatus for the study of surface chemistry routes to formation of complex organic molecules in space a new multi-beam apparatus for the study of surface chemistry routes to formation of complex organic molecules in space © @. *Review of Scientific Instruments*, 2020.
- [18] Mario Accolla. *Experimental Investigation on the Morphology of Interstellar Ice Analogues*. Theses, Université de Cergy Pontoise, April 2010.
- [19] S. E. Bisschop, G. W. Fuchs, E. F. van Dishoeck, and H. Linnartz. H-atom bombardment of HCOOH, CO₂ and CH₃CHO containing ices. In J. L. Lemaire and F. Combes, editors, *Molecules in Space and Laboratory*, page 62, December 2007.
- [20] B. M. Giuliano, R. M. Escrivano, R. Martín-Doménech, E. Dartois, and G. M. Muñoz Caro. Interstellar ice analogs: band strengths of H₂O, CO₂, CH₃OH, and NH₃ in the far-infrared region. , 565:A108, May 2014.

- [21] Joel R. Kimmel, Friedrich Engelke, and Richard N. Zare. Novel method for the production of finely spaced Bradbury-Nielson gates. *Review of Scientific Instruments*, 72(12):4354–4357, December 2001.
- [22] B. Schmitt, C. de Bergh, and M. Festou. *Solar system ices*, volume 227 of *Astrophysics and Space Science Library*. January 1998.
- [23] Harold I. Schiff. Neutral atmospheric chemistry — introduction and review. pages 85–98, 1973.
- [24] A. G. G. M. Tielens and W. Hagen. Model calculations of the molecular composition of interstellar grain mantles. , 114(2):245–260, October 1982.
- [25] Stephen P. Walch, Celeste Mc Michael Rohlfing, Carl F. Melius, and Charles W. Bauschlicher. Theoretical characterization of the minimum energy path for the reaction $\text{h}+\text{o}_2\rightarrow\text{ho}_2^*\rightarrow\text{ho}+\text{o}$. *The Journal of Chemical Physics*, 88:6273, 8 1988.
- [26] H. Koussa, M. Bahri, N. Jaïdane, and Z. Ben Lakhdar. Kinetic study of the reaction $\text{h}_2\text{o}_2+\text{h}\rightarrow\text{h}_2\text{o}+\text{oh}$ by ab initio and density functional theory calculations. *Journal of Molecular Structure: THEOCHEM*, 770:149–156, 9 2006.
- [27] F. Dulieu, L. Amiaud, E. Congiu, J. H. Fillion, E. Matar, A. Momeni, V. Pirronello, and J. L. Lemaire. Experimental evidence for water formation on interstellar dust grains by hydrogen and oxygen atoms. , 512:A30, March 2010.
- [28] Dapeng Jing, Jiao He, John Brucato, Antonio De Sio, Lorenzo Tozzetti, and Gianfranco Vidali. On Water Formation in the Interstellar Medium: Laboratory Study of the O+D Reaction on Surfaces. , 741(1):L9, November 2011.
- [29] Geoffrey A. Blake, E. C. Sutton, C. R. Masson, and T. G. Phillips. Molecular Abundances in OMC-1: The Chemical Composition of Interstellar Molecular Clouds and the Influence of Massive Star Formation. , 315:621, April 1987.
- [30] Nathalie Boudin, Willem A. Schutte, and J. Mayo Greenberg. Constraints on the abundances of various molecules in interstellar ice: laboratory studies and astrophysical implications. , 331:749–759, March 1998.
- [31] Kenzo Hiraoka, Tetsuya Sato, Shoji Sato, Norihito Sogoshi, Tatsuya Yokoyama, Hideaki Takashima, and Shinichi Kitagawa. Formation of Formaldehyde by the Tunneling Reaction of H with Solid CO at 10 K Revisited. , 577(1):265–270, September 2002.
- [32] Naoki Watanabe, Akihiro Nagaoka, Takahiro Shiraki, and Akira Kouchi. Hydrogenation of CO on Pure Solid CO and CO-H₂O Mixed Ice. , 616(1):638–642, November 2004.

- [33] G. W. Fuchs, H. M. Cuppen, S. Ioppolo, C. Romanzin, S. E. Bisschop, S. Andersson, E. F. van Dishoeck, and H. Linnartz. Hydrogenation reactions in interstellar CO ice analogues. A combined experimental/theoretical approach. , 505(2):629–639, October 2009.
- [34] H. Hidaka, M. Watanabe, A. Kouchi, and N. Watanabe. Reaction Routes in the CO-H₂CO-d_n-CH₃OH-d_m System Clarified from H(D) Exposure of Solid Formaldehyde at Low Temperatures. , 702(1):291–300, September 2009.
- [35] M. Minissale, A. Moudens, S. Baouche, H. Chaabouni, and F. Dulieu. Hydrogenation of co-bearing species on grains: unexpected chemical desorption of co. *Monthly Notices of the Royal Astronomical Society*, 458:2953–2961, 5 2016.
- [36] F. Dulieu, M. Minissale, and D. Bockelée-Morvan. Production of O₂ through dismutation of H₂O₂ during water ice desorption: a key to understanding comet O₂ abundances. , 597:A56, January 2017.
- [37] J. A. Noble, E. Congiu, F. Dulieu, and H. J. Fraser. Thermal desorption characteristics of CO, O₂ and CO₂ on non-porous water, crystalline water and silicate surfaces at submonolayer and multilayer coverages. , 421(1):768–779, March 2012.